Research

Characterization, surface preparation, conservation, and corrosion protection of bronze arrow heads from Cairo military museum using nanocomposite coating

Mohamed M. Megahed[1] · Noha H. Elashery[1] · Saleh M. Saleh[1] · A. M. El-Shamy[2]

Abstract

The study focused on examining approximately 32 arrowheads from Cairo's Qala Salah al-Din military museum, which showed significant signs of deterioration. The main objectives were to investigate the bronze alloy composition of these arrowheads and analyze the physical and chemical characteristics of their patinas. Understanding the causes and mechanisms of corrosion was crucial for developing effective conservation strategies to halt further degradation and identifying the corrosion products and metals involved. To achieve these goals, extensive examinations and analyses were conducted, including metallographic microscopy, SEM–EDS, and X-ray diffraction analysis to scrutinize the chemical composition, metallurgical features, and corrosion products of the bronze samples. Additionally, experimental studies were carried out to determine the most suitable protective coating for preventing future corrosion. Various combinations of ZnO nanoparticles with Paraloid® 48 or Paraloid® 66 coatings were tested on simulated arrowheads, and electrochemical techniques such as EIS and RP were employed for measurement. The results indicated that combining ZnO nanoparticles with either Paraloid® 48 or Paraloid® 66 coatings resulted in lower corrosion rates compared to using each coating alone. Based on these findings, chemical cleaning with ZnO nanoparticles and Paraloid® 48 was selected for treatment to protect the arrowheads' surfaces. Overall, this study provides valuable insights into preservation techniques for these historically significant artifacts.

Article Highlights

- Arrowhead Preservation: Nano-ZnO Coating Effective—Study reveals lower corrosion rates with ZnO and Paraloid® 48/66 combo.
- Bronze Arrowhead Conservation: Nano-ZnO Coating—Enhanced protection against corrosion observed in experimental tests.
- Historical Artifact Preservation: Nano-ZnO Coating—Findings inform conservation strategies for deteriorating arrowheads.

✉ A. M. El-Shamy, elshamy10@yahoo.com; am.elshamy@nrc.sci.eg | [1]Conservation Department, Faculty of Archaeology, Fayoum University, Faiyum, Egypt. [2]Physical Chemistry Department, Electrochemistry and Corrosion Lab., National Research Centre, El-Bohouth St. 33, Dokki, Giza 12622, Egypt.

Discover

1 Introduction

For millennia, bronze, an alloy of copper and tin, has been cherished for crafting a myriad of items, ranging from tools to intricate ornaments [1]. These artifacts not only hold cultural and historical significance but also captivate with their aesthetic appeal [2]. However, bronze is inherently prone to corrosion and deterioration, posing a significant challenge for preservation efforts [3]. Conservation of bronze artifacts requires a multifaceted approach, including preventive measures, treatment procedures, and ongoing vigilance [4]. One key preventive measure involves carefully regulating the storage environment to mitigate corrosion exacerbated by humidity, temperature fluctuations, and pollution [5, 6]. Equally important is the cautious handling and treatment of these fragile artifacts to prevent physical damage [7]. Treatment procedures such as cleaning and the application of protective coatings play a vital role in stabilizing and preserving bronze artifacts [8–12]. In some cases, more complex treatments like structural stabilization or electrochemical reduction may be necessary [13, 14]. Electrochemical reduction involves a process where chemical species gain electrons through electrochemical reactions, offering advanced conservation techniques [15–18]. It's essential to tailor these procedures to achieve specific goals and optimize reaction conditions [19]. Continuous monitoring through regular examinations and specialized equipment helps identify changes in artifact condition, prompting further treatment or preventive actions [20, 21]. In summary, bronze conservation is a dynamic process requiring a scientific understanding of materials, corrosion mechanisms, and a range of conservation techniques [22, 23]. Innovations such as climate-controlled storage, tailored cleaning methods, and advanced stabilization techniques aim to ensure the longevity of these valuable artifacts [24–26]. Some case studies demonstrate the use of nanocomposite coatings to conserve bronze artifacts effectively [27–29]. These coatings provide protection against corrosion and environmental factors while preserving the aesthetic and historical value of bronze objects [30].

1.1 Corrosion background

Understanding the corrosion background is pivotal for preserving bronze artifacts [31]. This involves a thorough exploration of the technical and scientific aspects related to corrosion in the context of bronze artifact conservation [32]. Bronze, primarily composed of copper (Cu) alloyed with tin (Sn), may contain other elements like zinc (Zn) and lead (Pb) [33–35]. Corrosion of bronze leads to the formation of patina, a complex layer of corrosion products on the artifact's surface [36, 37]. This corrosion process occurs electrochemically in the presence of moisture and oxygen, resulting in the oxidation of copper to form copper ions. Factors such as exposure to dissimilar metals, chlorides, and airborne pollutants can accelerate corrosion [38]. Initial corrosion produces cuprite, followed by the formation of tenorite and malachite, resulting in the characteristic green patina [39]. Higher humidity levels and airborne pollutants exacerbate corrosion, while rapid temperature changes can cause thermal stress [40]. Prolonged corrosion weakens the structural integrity of artifacts, leading to surface pitting and loss of detail. Removing corrosion products poses challenges, requiring a delicate balance between preservation and aesthetics [41]. Preventing ongoing corrosion involves identifying effective coatings or inhibitors and employing techniques like Electrochemical Impedance Spectroscopy (EIS) and Potentiodynamic Polarization to assess corrosion rates and mechanisms [42]. Analytical techniques such as X-ray diffraction (XRD) and scanning electron microscopy (SEM) aid in corrosion product analysis without damaging artifacts. Stabilizing the corrosion layer and applying protective coatings are essential for preventing further degradation [43]. Managing environmental conditions, such as temperature, humidity, light exposure, and pollutants, is crucial for artifact preservation [44]. Climate-controlled storage, protective coatings, and regular monitoring help mitigate corrosion risks. Implementing these strategies ensures the continued preservation of bronze artifacts for future generations [45]. The research objectives aim to address key aspects of the investigation comprehensively [46]. These include determining the elemental composition of bronze arrowheads, investigating surface preparation methods, developing nanocomposite coatings, evaluating their effectiveness through electrochemical techniques, and providing practical recommendations for conservators [47]. By structuring research objectives in this manner, the study can effectively tackle the challenges associated with bronze artifact conservation and protection using nanocomposite coatings [48].

2 Materials and methods

We meticulously curated the data for our study following a predefined experimental protocol aimed at capturing the pertinent parameters affecting bronze corrosion under specified conditions. Our selection criteria prioritized factors such as reproducibility, consistency, and relevance to our research objectives [49]. Each experiment was conducted with a strong emphasis on reproducibility to bolster the reliability of our findings. Key experiments were repeated multiple times to ensure statistical significance and to address variability, with the specific number of repetitions determined by the nature of the experiment and associated statistical considerations. Our dedication to scientific rigor compelled us to replicate experiments to validate results and confirm the consistency of observed trends [50]. We implemented rigorous quality control measures throughout the experimental process to minimize experimental errors and enhance the precision of our data. Calibration procedures, standardization of experimental conditions, and adherence to established protocols were fundamental components of our methodology. We uphold transparency in scientific inquiry by providing detailed descriptions of the experimental setup, procedures, and data analysis in the methods section of our published paper.

2.1 Description and condition

Bronze, an alloy composed of copper, tin, and other trace elements, has played a pivotal role in the crafting of weaponry across different epochs. These weapons, diverse in size and design, have left an indelible mark on history. While each weapon may inflict varying forms of damage, the common outcome is the act of severing or truncating. In this pursuit of understanding, researchers embarked on an investigation of approximately 33 arrowheads showcased at the Military Museum of Salah al-Din al-Ula. The aim was to unravel the secrets concealed within these artifacts and gain deeper insights into their historical significance and craftsmanship (Figs. 1, 2a–e).

Table 1 offers a visual representation of the arrowhead group, presenting insights into their various characteristics, including weight, dimensions, and sizes, created using Adobe Illustrator 2020. This discussion explores the significant observations and implications drawn from this dataset. The arrowheads display a notable range in weight, ranging from 2 to 6 g, indicating potential differences in design, materials, or intended uses. Particularly, Arrow no. 19 stands out with its weight of 6 g, suggesting distinct design or usage compared to the others. Examination of length and width dimensions further highlights the diversity within the arrowhead collection. Length varies from 2 cm to 4.4 cm, while width ranges from 0.7 cm to 1.15 cm. These size discrepancies may indicate specialized arrowhead types tailored for specific purposes or associated with historical contexts. Arrow no. 11, with its above-average width of 1.15 cm, raises the possibility of a unique design or application. A comparison between photographic and diagrammatic representations reveals both similarities and significant differences in dimensions among the arrowheads, suggesting the presence of distinct designs within the collection. The data presented in Table 1 underscores the importance of examining the diverse physical attributes of these arrowheads, shedding light on potential typologies, chronological sequences, or cultural variations in their production and usage. Additionally, understanding these attributes contributes to discussions regarding their aerodynamic properties, which may further illuminate their effectiveness as tools. In summary, Table 1 serves as a foundational reference for ongoing analyses in this study. The wide range of weights, dimensions, and sizes among the arrowheads sparks curiosity about their cultural significance, potential implications, and technological advancements of their era. This comprehensive examination deepens our understanding of these artifacts and provides valuable insights into the craftsmanship and contextual factors influencing their creation and use.

2.2 Physio-chemical characterization

The investigation of these artifacts involved employing a diverse range of techniques for both physical and chemical analysis. This comprehensive approach encompassed X-ray diffraction, scanning electron microscopy with energy dispersive spectroscopy (SEM&EDS), and metallographic microscopy. SEM&EDS played a pivotal role in offering precise insights into the chemical composition of the arrowheads, providing valuable information about their makeup [51]. Conversely, X-ray diffraction delved into the composition of the metal/alloy used in their construction and offered insights into the corrosion products, aiding in our understanding of burial conditions. Metallographic microscopy focused on assessing the microstructure of the arrowheads and examining surface corrosion. These varied analytical methods synergized to comprehensively describe the materials and provide a thorough physical and chemical characterization of the objects.
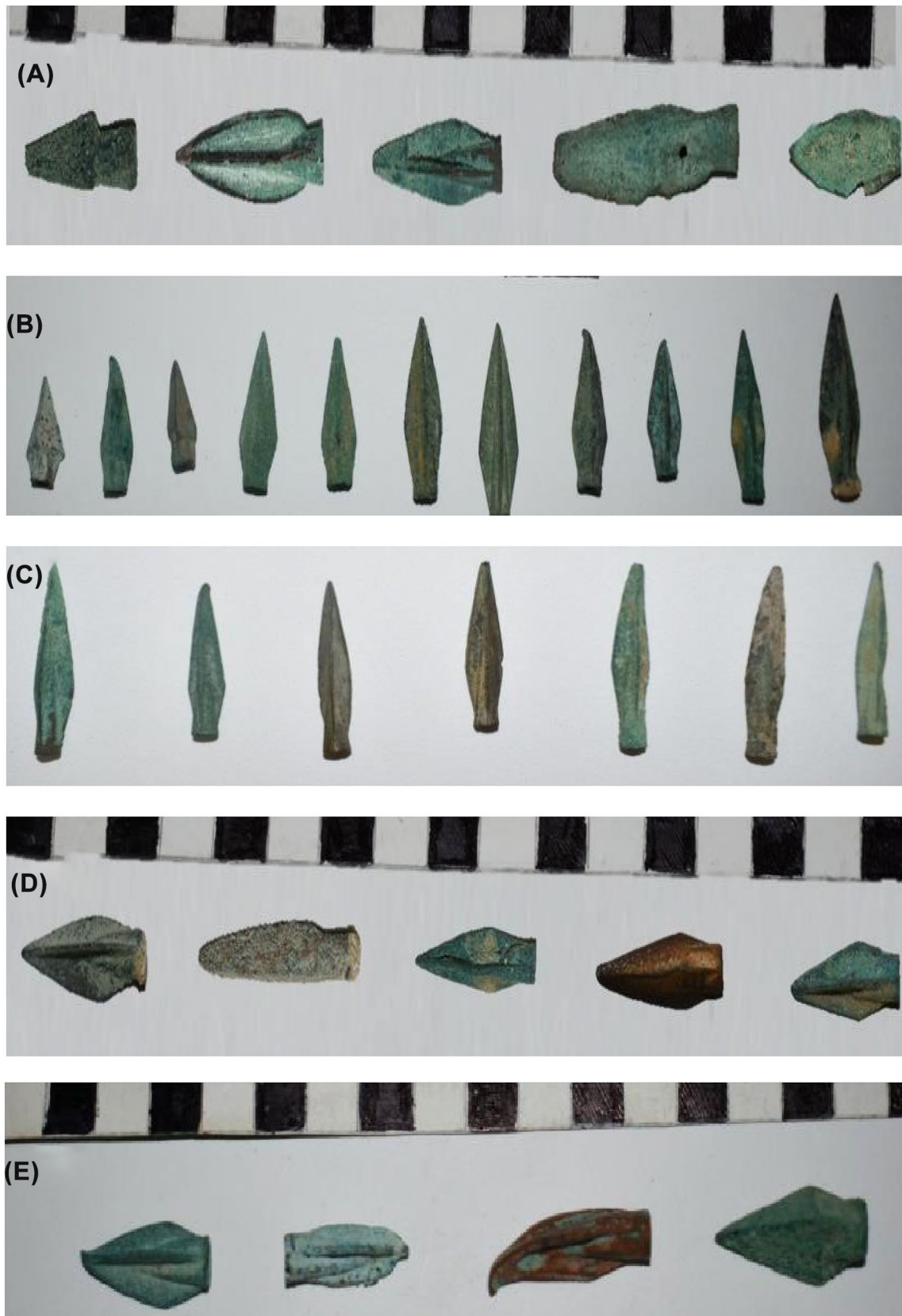
Fig. 1 **a**, **b**, **c**, **d**, and **e** Show the images of collective arrowheads before the treatment showing the different deterioration aspects
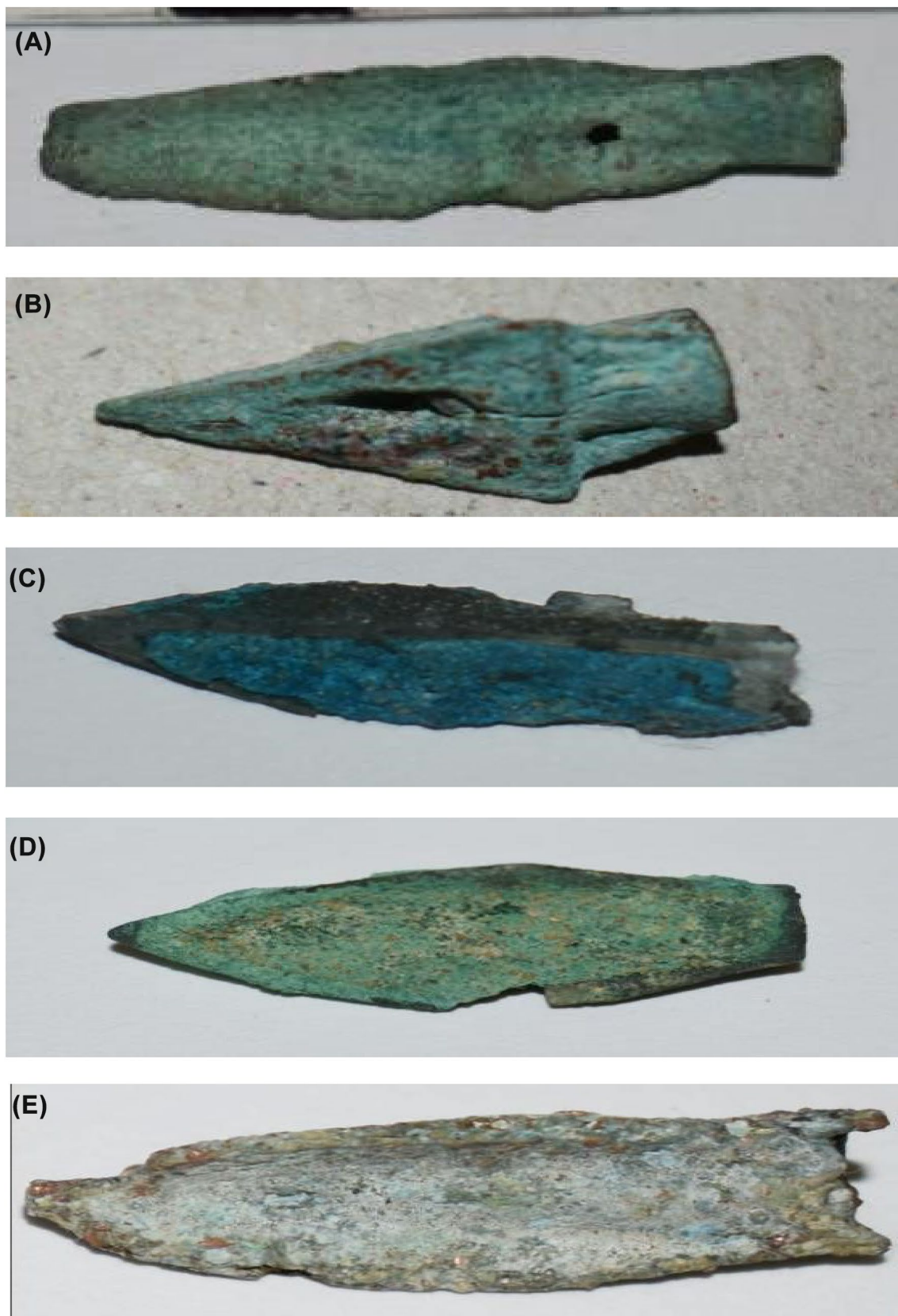
Fig. 2 **a**, **b**, **c**, **d**, and **e** Show the images of individual arrowheads before the treatment and it is noticed they suffered from different deterioration aspects, **f** Shows a geometric drawing for the group of arrowheads showing their different dimensions and sizes. **a**–**d** represent group 1 (pale green/brown corrosion) and **e** represents group 2 which fall under (rust-colored black and brown corrosion)
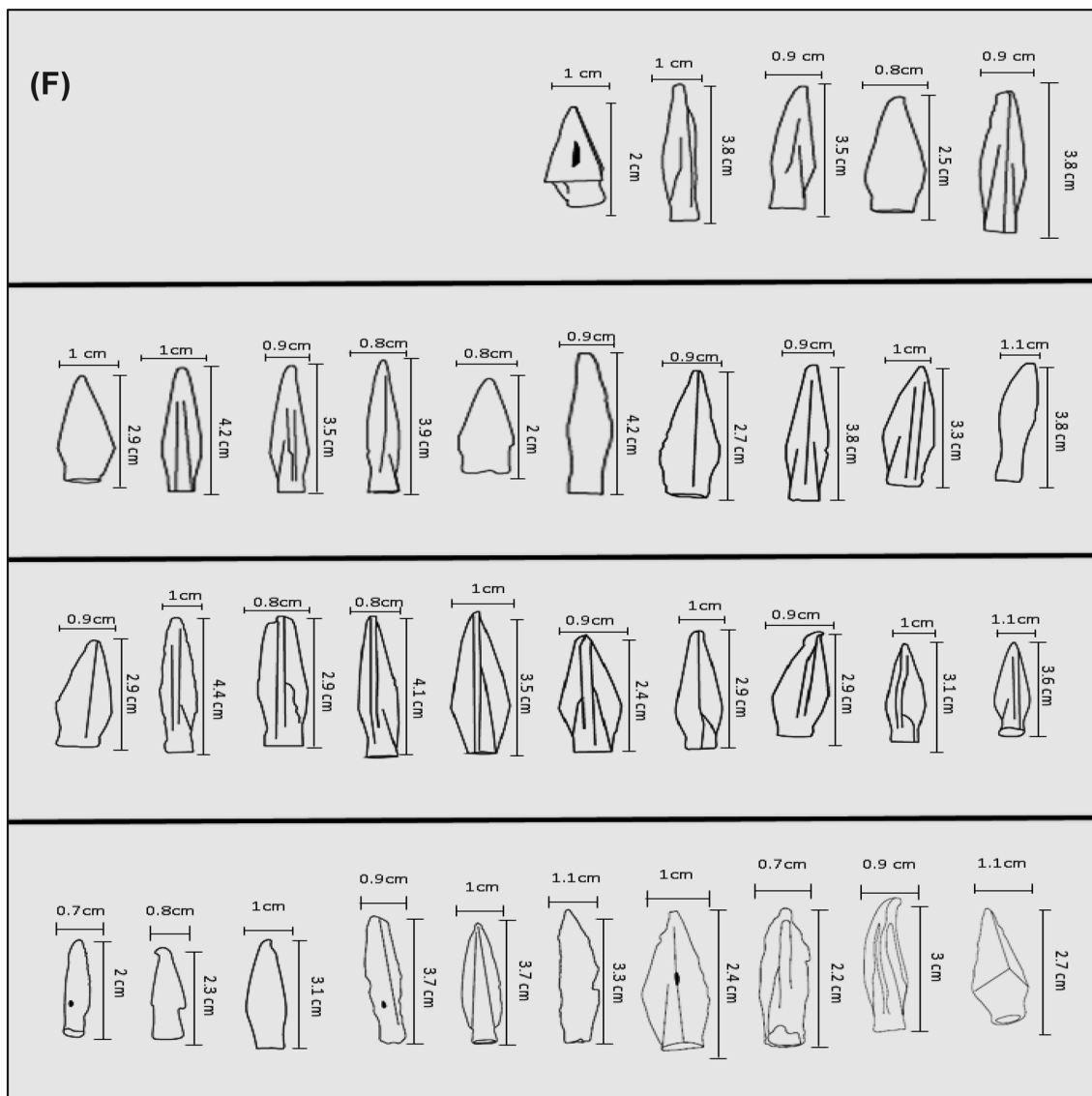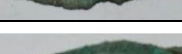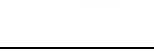
Fig. 2 (continued)

In essence, this multifaceted approach to analysis, incorporating metallographic microscopy, SEM&EDS, and X-ray diffraction, facilitated a detailed examination of the arrowheads, shedding light on their composition, corrosion, and burial history [52].

2.2.1 Metallographic examination (ME)

Achieving a polished surface on bronze requires a stepwise process using increasingly finer grits of sandpaper. Initial sanding begins with coarse-grit sandpaper, such as 80 or 100 grit, to remove prominent imperfections or old coatings. Progress to medium-grit sandpaper, around 150 or 180 grit, to further smooth the surface and reduce scratches. Fine sanding involves using fine-grit sandpaper, like 220 or 320 grit, to refine the surface and eliminate finer scratches. For extra fine sanding, switch to sandpaper in the range of 400 to 600 grit to achieve a smoother and more polished appearance. Very fine sanding can be achieved with sandpaper typically ranging from 800 to 1200 grit to minimize visible scratches and enhance smoothness. Finally, for ultra-fine sanding, use sandpaper ranging from 1500 to 2000 grit to contribute to the development of a glossy surface with minimal imperfections. Optionally, move on to polishing compounds or abrasives beyond 2000 grit to achieve a reflective, mirror-like finish. Maintain a consistent sanding motion, whether circular or linear, to avoid uneven surfaces. Gradually progress through finer grits to achieve a smoother finish, removing

Table 1 Shows a geometric drawing of the group of arrowheads showing their different weights, dimensions, and sizes

Arrow no.	Width, cm	Length, cm	Weight, g	Diagram	Photo
1	1.1	2.7	5.0		
2	0.9	3.0	2.0		
3	0.7	2.2	2.0		
4	1.0	2.4	2.0		
5	1.1	3.3	4.0		
6	1.0	3.7	2.0		
7	0.9	3.7	5.0		
8	1.0	3.1	2 g		
9	0.8	2.3	3.0		
10	0.7	2.0	3.0		
11	1.15	3.6	3.0		
12	1.04	3.1	2.0		
13	0.97	2.9	2.0		

any residue between grit changes to prevent contamination and ensure effective sanding. Wet sanding with water or a lubricant can enhance the effectiveness of finer grits. By following this grit sequence and incorporating these tips, you can effectively attain a mirror-like surface on bronze arrowheads or similar artifacts. A comprehensive metallographic

Table 1 (continued)
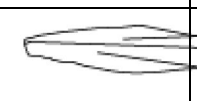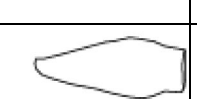
14	1.04	2.9	5.0		
15	0.94	2.4	2.0		
16	1.09	3.5	4.0		
17	0.88	4.1	2.0		
18	0.85	2.9	2.0		
19	1.0	4.4	6.0		
20	0.98	2.9	5.0		
21	1.10	3.8	5.0		
22	1.06	3.3	4.0		
23	0.93	3.8	4.0		
24	0.94	2.7	3.0		
25	0.94	4.2	5.0		
26	0.85	2.0	2.0		

Table 1 (continued)

27	0.83	3.9	4.0		
28	0.94	3.5	4.0		
29	1.05	4.2	5.0		
30	1.07	2.9	6.0		
31	0.92	3.8	5.0		
32	0.88	2.5	3.0		

examination was conducted to gain deeper insights into the metal composition of the arrowheads and the processes leading to surface deterioration. This research aimed to uncover intricate details about the production techniques and technologies employed in their creation. However, accessing this valuable data required an intrusive approach, which involved carefully removing tiny sections from the arrowheads and embedding them to create cross-sections for analysis. Subsequently, these samples underwent meticulous processing. They were mounted, polished using silicon carbide sheets, degreased with ethanol, and rinsed with distilled water. Following these preparatory steps, the samples were immersed in an aqueous solution of ferric chloride, serving as an etching reagent, and then gently dried with a clean towel. Subsequently, the prepared samples were examined under a metallographic microscope for further analysis (refer to Fig. 3). Despite the somewhat intrusive nature of this method, the metallographic analysis yielded crucial insights into the arrowheads and their production process. This included valuable information about the quality of materials used and the techniques employed during their creation. The metallographic examination of arrowhead samples not only unveiled the microstructure of the metal but also helped identify signs of deterioration scattered across the metal surface. This meticulous examination provided significant revelations regarding both the quality of the materials used in crafting the arrowheads and the invaluable insights into the techniques employed in their fabrication [53]. The preparation of samples for corrosion experiments involves several critical steps, including cutting, sizing, and ensuring proper sample quality. Choose representative bronze arrowheads from the collection, ensuring they exhibit typical corrosion patterns and are suitable for analysis. Use a precision cutting tool or equipment to section the arrowheads carefully, avoiding additional defects or alterations to the structure. The aim is to obtain sections showcasing both the corroded surface and the interior structure of the bronze. After cutting, use abrasive materials or grinding tools to smooth the cut surfaces, gradually progressing through finer abrasives to achieve a polished finish. Thoroughly clean the samples to remove any debris, dust, or contaminants introduced during cutting and grinding, using solvents or cleaning agents that do not interfere with subsequent analyses. Document details related to each sample, including origin, cutting date, and specific features observed during preparation, to ensure traceability. Store the prepared samples in a controlled environment to prevent further corrosion or contamination, considering replicating the preparation process for multiple samples to ensure reliability and reproducibility of the experimental results. By following these steps, you can prepare bronze arrowhead samples for corrosion experiments, ensuring they are representative, well-prepared, and suitable for in-depth analysis of corrosion mechanisms and protection strategies [54]. Understanding the findings related to pits and crevices corrosion in metallographic examination (Fig. 3) pictures of the bronze samples involves a detailed examination of the microstructure and surface features using a metallographic microscope. This allows for high-resolution imaging of the
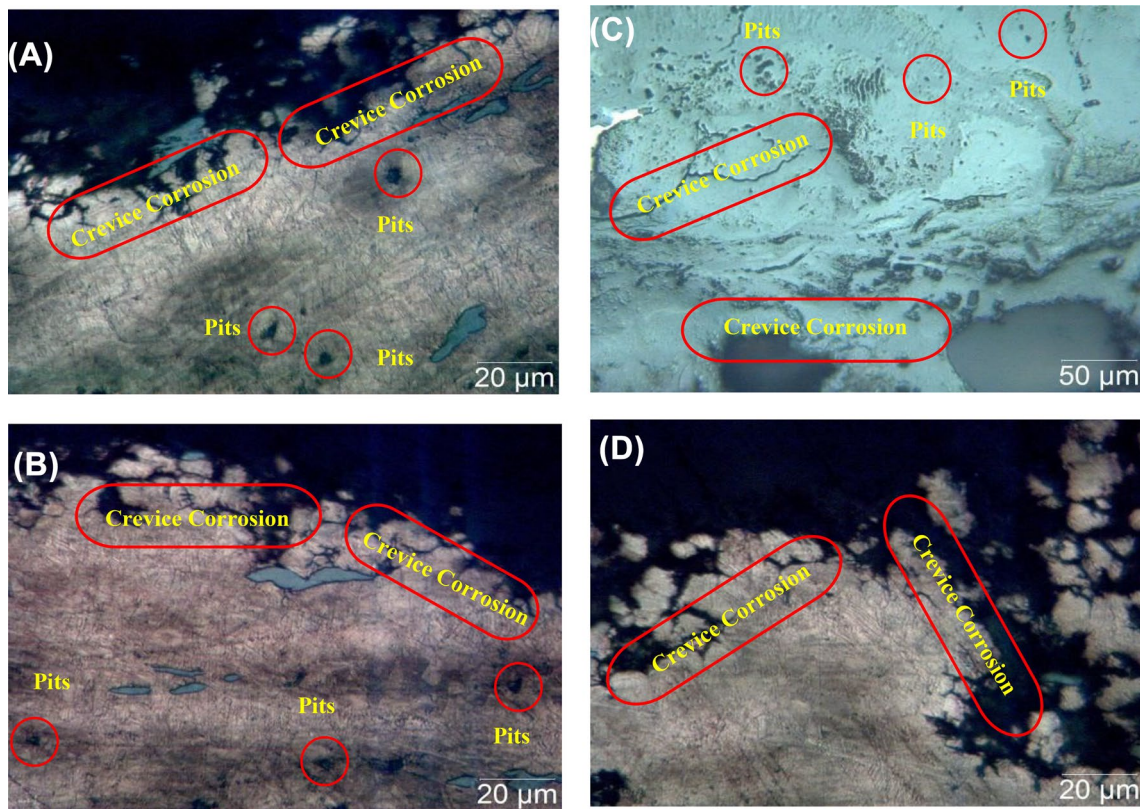
Fig. 3 ME ex., for a sample from the arrowheads, shows **a** the localized attack (pitting corrosion). **b** the pitting corrosion propagation and dispersed on the alloy surface. **c** the micro-cracks disturbing the alloy surface. **d** the crevice corrosion dispersed on the alloy surface

sample's surface and internal structure, identifying localized areas exhibiting distinct features such as pits and crevices. Analyze the morphology of these corrosion features to understand their shapes, sizes, and distribution, considering factors like depth and extent. Examine the corrosion products within and around pits and crevices, assessing the severity and identifying any correlations with specific regions or phases in the bronze alloy [55]. Variations in alloy composition can influence localized corrosion susceptibility, particularly along grain boundaries. Understanding pits and crevices corrosion provides valuable insights into localized corrosion behavior, crucial for formulating effective conservation and protection strategies to mitigate further deterioration.

2.2.2 Scanning electron microscope and energy dispersive spectrometry (SEM&EDS)

The study discusses a scientific investigation that involved collecting two samples from arrowheads, followed by examination using an electron microscope equipped with an energy dispersive unit. The main aim was to explore the microstructure, chemical composition, and erosion sites on these arrowheads [56]. The analysis utilized a scanning electron microscope (SEM) and energy-dispersive X-ray spectroscopy (EDS) to scrutinize the materials. An FEI Inspect S 50 microscope with a Bruker AXS-Flash Detector 410-M attachment was used for this purpose. The results of the analysis are presented visually in Figs. 4 and 5, along with summarized data in Table 2, showcasing images, scans, and identified objects with their characteristics [57]. The arrowheads were systematically categorized into two groups based on their corrosion product characteristics [58]. The first group exhibited thick corrosion products with a pale green/brown coloration, while the second group displayed rust-colored black and brown corrosion, often accompanied by small fragments, and scattered pale green areas. Samples from each group were selected for SEM&EDS examination, which was conducted using an Inspect S50 instrument by FEI with specific parameters. The examination provided critical details about the arrowhead samples, revealing their microstructure, deteriorated areas, and chemical composition [59]. It's crucial to clarify the criteria used for sample categorization and selection in the study to ensure transparency and a comprehensive understanding. Visual observation of corrosion products was the primary criterion for categorizing and selecting samples for further analysis, as these products offer visible indications of the artifacts' degradation state. Two distinct groups were identified
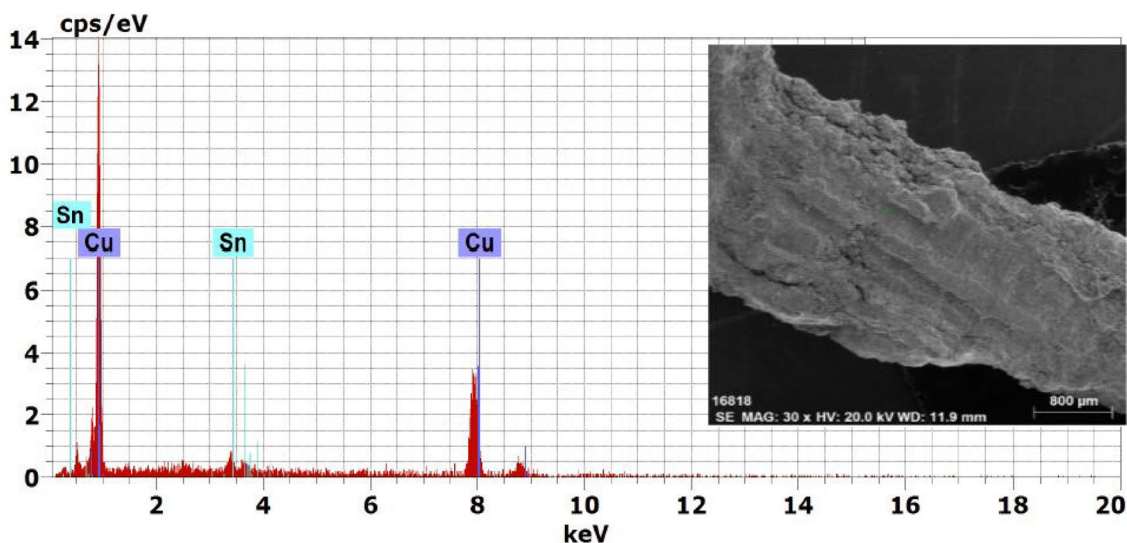
Fig. 4 Shows SEM&EDS ex., for a sample from the arrowhead, the photo shows the deterioration of the alloy, and the SEM&EDS scan shows the elemental composition of the arrowheads
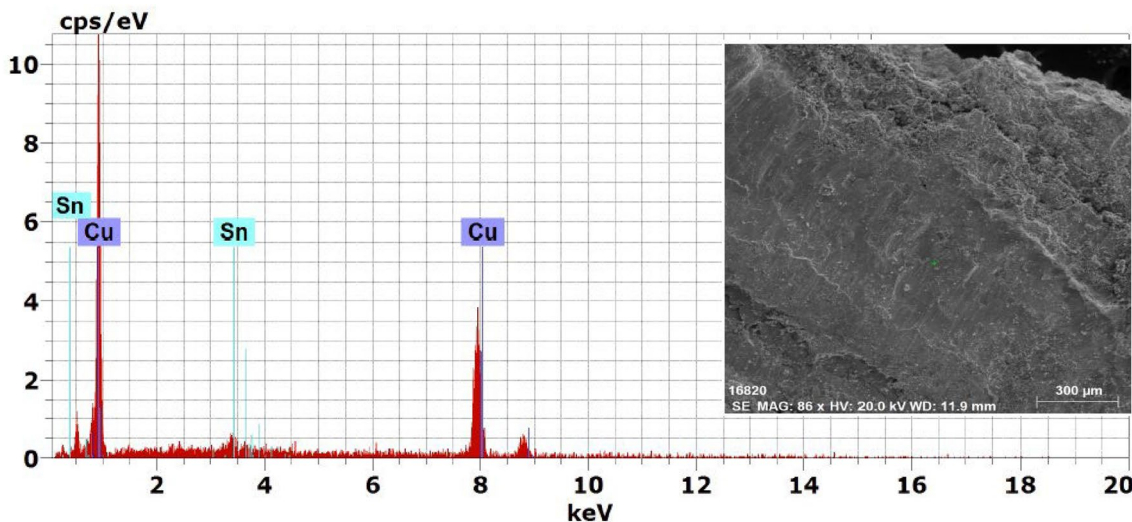
Fig. 5 Shows SEM&EDS ex., for a second sample from the arrowheads, the photo shows the appearance of the rough surface closely and the calcified rust layers and SEM&EDS Scan shows the elemental composition of the arrowheads

Table 2 Shows SEM&EDS analysis results for two samples from the arrowheads	Samples	Elements		
		Cu%	Sn%	Total%
	No.1	90.10	9.90	100.00
	No.2	92.17	7.83	100.00

based on the visual characteristics of corrosion products observed on the arrowheads' surfaces. The selection process considered overall corrosion patterns, including the nature, distribution, and intensity of corrosion products [60]. Different corrosion patterns were associated with each group, guided by previous studies on bronze corrosion and degradation patterns. Efforts were made to avoid sample bias by ensuring diverse representation of corrosion states within the artifact collection. The categorization criteria also considered historical context, artifact location, and known material characteristics. Detailed documentation of these factors ensures a comprehensive understanding of the sample selection

Discover

process, adhering to conservation ethics to preserve the integrity of historically significant artifacts. The categorization based on visual observations influenced subsequent analyses and conservation strategies, emphasizing a transparent and systematic approach to sample selection.

Table 2 displays the outcomes of the SEM&EDS examination performed on two distinct samples extracted from different arrowheads, offering detailed information about their elemental composition. These results are significant as they furnish valuable insights into the arrowhead manufacturing process, the materials utilized, and their potential implications for historical metallurgy and craftsmanship. In this analysis, we will explore the interpretation and importance of the elemental percentages depicted in Table 2. The elemental makeup of the first sample, identified as No.1, indicates a prominent copper content of 90.10%. This substantial presence of copper strongly indicates that the arrowhead was primarily fashioned from a copper-based alloy, consistent with historical practices where copper's abundance and malleability made it a prevalent choice for metalwork. The inclusion of 9.90% tin suggests the potential use of a bronze alloy, amalgamating the desirable properties of both copper and tin. Notably, the absence of elements like lead, iron, sulfur, and antimony suggests a relatively pure copper-tin composition in this particular arrowhead sample. Likewise, the second sample, denoted as No.2, demonstrates a high copper percentage of 92.17%. This reaffirms the common application of copper-based alloys in arrowhead production during the historical period in question. The presence of 7.83% tin further supports the inference of a bronze alloy, highlighting the significance of this alloy in historical metallurgy. Once again, the lack of additional elements emphasizes the notion of a relatively straightforward copper-tin alloy composition. The consistent elemental composition observed in both samples underscores the exceptional metallurgical proficiency of the era. The deliberate selection and adept combination of these materials reflect the artisans' expertise in manipulating available resources to achieve desired qualities in their final products. These findings align seamlessly with existing archaeological knowledge of ancient metallurgy, where the utilization of copper and its alloys played a pivotal role in crafting various tools and weapons. The reliance on copper-based alloys, particularly bronze, exemplifies the ingenuity of ancient metalworkers, enabling them to create functional and long-lasting artifacts. In summary, the SEM&EDS analysis outcomes presented in Table 2 offer valuable insights into the elemental composition of the examined arrowhead samples. The prevalence of copper and the presence of tin in both samples correspond with established historical metallurgical practices. This data serves as a tangible link to the past, illuminating the specific materials and techniques employed by skilled artisans to craft these arrowheads. A deeper comprehension of these elemental details significantly contributes to our broader understanding of the historical context, metallurgical expertise, and craftsmanship inherent in these remarkable artifacts.

2.2.3 X-ray diffraction analysis (XRD)

An examination was conducted to determine the composition of corrosion byproducts found on arrowhead surfaces. X-ray diffraction (XRD) analysis, utilizing Cu Kα radiation and a Philips X-Ray Diffractometer (model pw1840), was employed on arrowheads collected in two distinct sets. The main objective was to identify corrosion compounds and evaluate their reliability, durability, and suitability for conservation purposes [61]. This knowledge is crucial for making informed decisions regarding the appropriate storage and display conditions for these artifacts. The results of this analysis are presented in Figs. 6, 7, with specific compounds detailed in Table 3. The primary focus of this investigation was to gain a precise understanding of the composition of corrosion products, enabling informed decisions regarding conservation. Arrowheads were categorized into two groups based on their corrosion characteristics, and samples from each group underwent analysis using the Philips X-Ray Diffractometer. This analysis facilitated the identification of corrosion compounds and assessment of their authenticity, stability, and suitability for treatment. Such information serves as a valuable guide for preservation and display decisions [62]. Deciphering the composition of corrosion products allows for the formulation of strategic preservation methods, aligning with the goal of safeguarding the historical significance of these artifacts. Table 3 provides a comprehensive overview of the results obtained from XRD analysis, focusing on the corrosion products found on the examined arrowheads. This analysis yields valuable insights into the chemical compounds formed as a result of the corrosion process [63]. The corrosion products from the first sample reveal the presence of Antlerite and Paratacamite as the primary major compounds, indicating significant copper involvement in the corrosion process. The identification of Brochantite and Malachite further emphasizes the presence of copper compounds and carbonates. Similarly, the corrosion products from the second sample also feature

Fig. 6 Shows XRD scan for the corrosion products of the first group of arrowheads
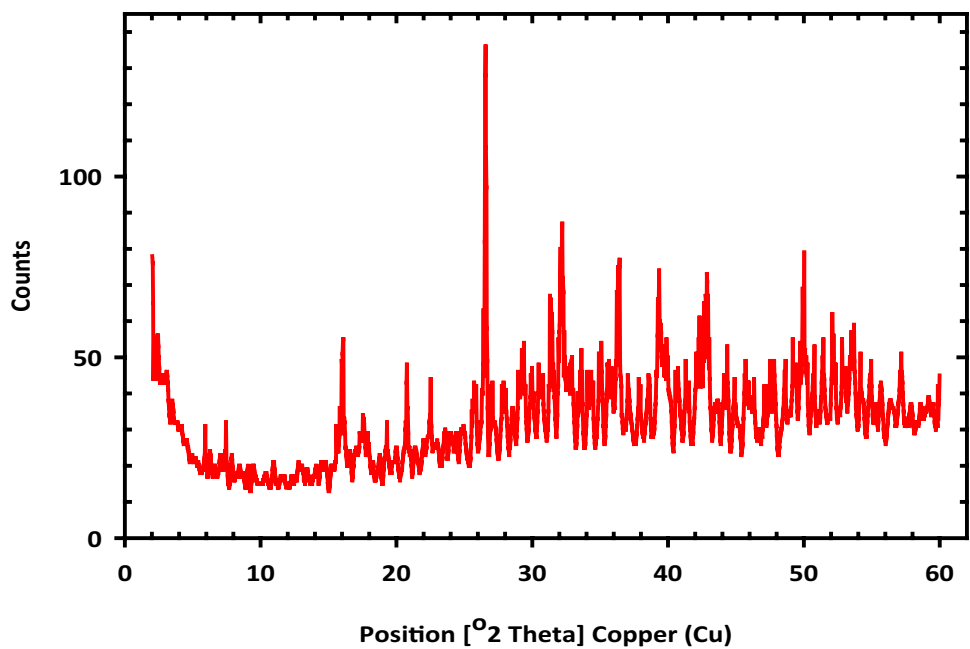
Fig. 7 Shows XRD scan for the corrosion product of the second group of arrowheads
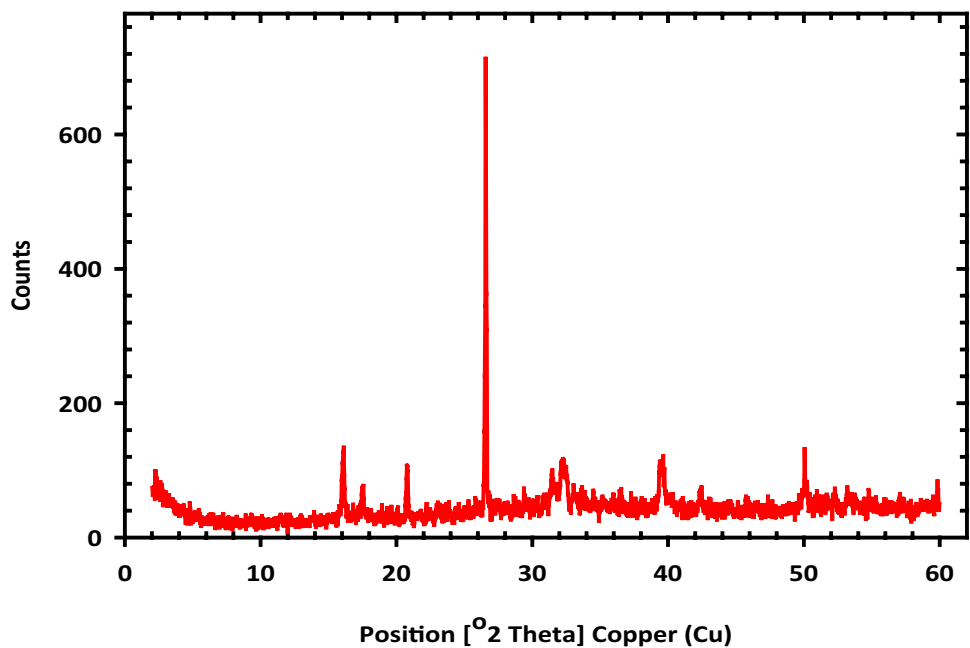
Table 3 Shows the XRD analysis results of the corrosion products of the arrowheads

Samples	Compounds				
	Essential major (Above 60%)	Major (40:60)	Minor (10:40)	Small Minor (5:10%)	Traces(1:5%)
The first sample	–	Antlerite $Cu_3(SO_4)(OH)_4$ Paratacamite $Cu_2(OH)_3Cl$	Brochantite $CuSO_4.3Cu(OH)_2$	Malachite $CuCO_3\ Cu(OH)_2$	–
The second sample	–	Antlerite $Cu_3(SO_4)(OH)_4$ Paratacamite $Cu_2(OH)_3Cl$	Brochantite $CuSO_4.3Cu(OH)_2$ Quartz SiO_2	Malachite $CuCO_3\ Cu(OH)_2$	–

Discover

Antlerite and Paratacamite as essential major compounds, along with Brochantite, Quartz, and Malachite, indicating interactions between copper compounds and silicate minerals [64]. The prevalence of copper-based minerals in the corrosion products underscores the complex interaction between the arrowheads' material composition and environmental conditions. Understanding these corrosion products is instrumental in devising appropriate conservation strategies to prevent further deterioration and provides valuable insights into the arrowheads' historical context and preservation requirements. In conclusion, the XRD analysis results offer valuable insights into the corrosion products present on the arrowheads, enriching our understanding of their historical journey and preservation needs [65]. Analyzing XRD results involves attributing diffraction peaks to specific crystallographic phases present in the sample. To identify components like Antlerite, Paratacamite, Brochantite, Malachite, and Quartz, characteristic peak positions (2θ values) and relative intensities associated with each phase must be considered. Reference databases and software tools can aid in this analysis, helping to confirm the presence of specific minerals in the samples. Additionally, factors like crystallinity and peak width provide further information about sample composition and crystal structure, contributing to a comprehensive analysis.

2.3 Preparation of the coatings

The coating compositions were developed by combining Paraloid® 48, Paraloid® 66, and ZnO nanoparticles, selected for their known properties and potential impact on bronze corrosion behavior. In the initial step, precise quantities of each component were weighed using analytical balances to achieve the desired composition, ensuring consistency. The next step involved selecting an appropriate solvent (ethanol was used in this study) to dissolve the components and create a homogeneous solution, chosen based on compatibility and evaporation characteristics. Following solvent selection, thorough mixing and homogenization were performed using magnetic stirring to ensure even distribution of particles and molecules within the solution. Subsequently, the prepared coating solution was applied to the bronze specimens using brush coating to attain a uniform and controlled coating thickness. Finally, the coated specimens were left to dry under controlled conditions (at room temperature for 24 h) to facilitate solvent evaporation and ensure proper adhesion of the coating to the bronze surface. Careful control of coating thickness was maintained to ensure uniformity across all samples, with an average thickness of approximately 50 μm.

2.4 Electrochemical measurements

Performing electrochemical measurements for bronze corrosion involves a series of steps and techniques. Firstly, sample preparation entails obtaining a representative bronze sample free from contaminants. Thorough cleaning, either through ultrasonic cleaning or abrasive polishing, exposes a clean surface for electrochemical measurements. Subsequently, the sample is rinsed with distilled water and dried under nitrogen to prevent oxidation. The electrochemical cell setup involves preparing a three-electrode system consisting of a working electrode (bronze sample), a reference electrode (silver/silver chloride), and a counter electrode (platinum electrode). Proper sealing of the cell is crucial to prevent external interference. For electrolyte preparation, an electrolyte solution mimicking the corrosion environment, often NaCl solutions for marine environments, is chosen. High-purity reagents and deionized water are used to prepare the solution. Open circuit potential (OCP) measurements involve recording the potential of the bronze sample immersed in the electrolyte solution after stabilization. Tafel analysis entails performing Tafel polarization measurements to investigate corrosion kinetics by applying potential perturbations and measuring resulting currents. Potentiodynamic polarization scans sweep the potential over a specified range at a controlled scan rate to understand corrosion behavior and identify critical potentials. Electrochemical impedance spectroscopy (EIS) involves applying small amplitude AC voltage to record impedance spectra for studying corrosion processes at different frequencies. After experiments, data analysis involves interpreting collected data to conclude bronze corrosion behavior under specific conditions. A comprehensive report documenting experimental parameters, methodologies, and results, including graphs and tables, is essential. Regarding the selection of a potential for potentiostatic polarization measurements, a potential of 0.0 V vs Ag/AgCl was chosen to approximate the onset of passivation and capture early stages of passivation, providing insights into the passive layer's effectiveness. Monitoring pH variations upon adding sulfide ions to the electrolyte solution involved systematic pH measurements. Sulfide ions were sourced from sodium sulfide (Na_2S), and a stock solution was prepared by dissolving Na_2S in distilled water. Careful control of concentration and observation for precipitation ensured reproducibility and accuracy in corrosion studies.

3 Electrochemical techniques

3.1 Open circuit potential

The use of open circuit potential (OCP) curves is a well-established method for examining the corrosion behavior of metals and alloys in various environments [66]. In this study, OCP curves are employed to investigate how the presence of ZnO nanoparticles affects the corrosion kinetics of bronze immersed in a 3.5% NaCl solution containing either 2% Paraloid® 48 or Paraloid® 66 [67]. Bronze, primarily consisting of copper with added tin and other alloying elements, is known for its inherent resistance to corrosion, although certain conditions can still make it susceptible. Exposure to sodium chloride (NaCl) solutions, for instance, poses a significant corrosion risk to bronze [68]. The main objective here is to use OCP curves to evaluate whether incorporating ZnO nanoparticles can improve the protective properties of Paraloid® 48 and Paraloid® 66, which are commonly used acrylic resin coatings for corrosion prevention on metal surfaces. OCP curves enable the tracking of potential differences between the bronze specimen and a reference electrode over time when exposed to the NaCl solution, with variations in coatings containing or lacking ZnO nanoparticles [69]. A more negative potential reading indicates increased corrosion activity, while a more positive potential suggests improved resistance to corrosion as seen in Fig. 8. If the addition of ZnO nanoparticles proves effective in enhancing coating protection, the OCP curves will show more positive potentials for bronze samples treated with ZnO compared to those without. This shift in potential would signify reduced corrosion activity and improved coating effectiveness in preventing corrosion [70]. Overall, OCP curves serve as a valuable tool for assessing the performance of coatings and determining the potential benefits of incorporating ZnO nanoparticles to strengthen their protective properties in a NaCl solution environment [71]. This investigation significantly contributes to our understanding of corrosion prevention strategies for bronze artifacts and other metal surfaces [72].

Fig. 8 Open circuit potential curves represent the effect of adding ZnO nanoparticles on the corrosion behavior of bronze in 3.5% NaCl solution containing **A** 2% Paraloid® 48 and **B** Paraloid® 66
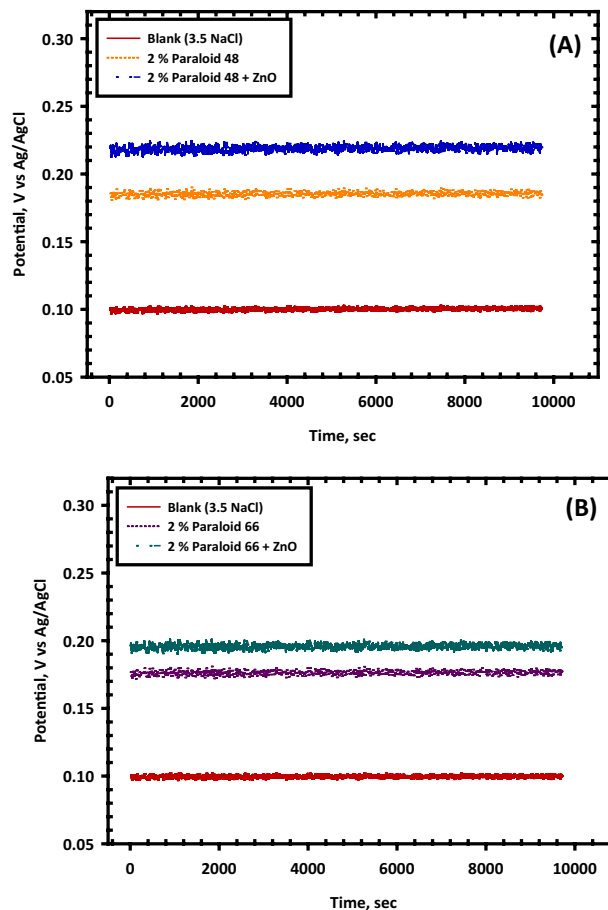
Fig. 9 Polarization curves represent the effect of adding ZnO nanoparticles on the corrosion behavior of bronze in 3.5% NaCl solution containing. **A** 2% Paraloid® 48 and **B** Paraloid® 66
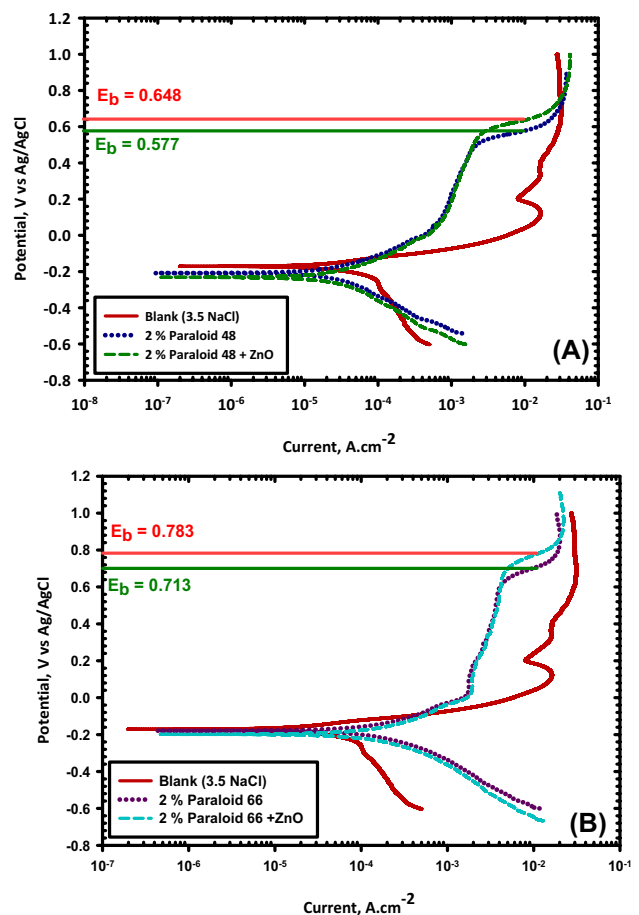
3.2 Potentiodynamic polarization technique

As previously mentioned, polarization curves are a widely used method for examining the corrosion tendencies of metals in various environmental conditions. These curves illustrate the relationship between anodic and cathodic current densities concerning the applied potential [73]. By analyzing polarization curves, essential electrochemical parameters such as corrosion potential, corrosion rate, and more can be determined. When considering bronze immersed in a 3.5% NaCl solution containing either 2% Paraloid® 48 or Paraloid® 66, the introduction of ZnO nanoparticles can significantly influence corrosion behavior. ZnO is known for its effective corrosion inhibition properties, attributed to its ability to form a protective layer on the metal surface [74]. Incorporating ZnO nanoparticles into the solution with Paraloid® 48 leads to an observable shift in the polarization curve towards the left, indicating a reduction in corrosion current density. This shift suggests that the addition of ZnO nanoparticles positively affects bronze corrosion behavior in this environment. It implies that the ZnO nanoparticles act as cathodic inhibitors, decreasing the rate of the cathodic reaction and thus reducing the overall corrosion rate [75]. Paraloid® is a thermoplastic resin commonly used in coatings and adhesives, with Paraloid® 48 and Paraloid® 66 representing distinct grades of this resin. Paraloid® 48 consists of a copolymer blend of methyl methacrylate and ethyl acrylate, while Paraloid® 66 is a terpolymer composed of methyl methacrylate, ethyl acrylate, and methacrylic acid [76]. Incorporating ZnO nanoparticles into bronze in the presence of Paraloid® can significantly influence corrosion behavior due to the nanoparticles' ability to serve as a barrier, preventing the infiltration of corrosive elements such as chloride ions to the bronze surface [77]. The polarization curves obtained for bronze in the presence of Paraloid® and ZnO nanoparticles offer valuable insights into the material's corrosion behavior by measuring current density as a function of the applied potential as illustrated in Fig. 9 [78]. Analyzing the potentiostatic results is crucial for connecting them to the study objectives and providing a meaningful interpretation of the findings. Our focus was primarily on understanding the behavior of the passive film formed on the bronze surface under various experimental conditions. This investigation is essential for achieving our study objectives, which aim to elucidate corrosion

mechanisms and evaluate the efficacy of surface treatments in enhancing bronze corrosion resistance [79]. The potentiostatic experiments allowed us to maintain a constant potential on the bronze samples and observe the response of the passive film over time. Choosing a potential of 0.0 V vs Ag/AgCl aimed to capture the onset of passivation and the early stages of passive film formation. One significant outcome of the potentiostatic measurements is the clear differentiation in passive film behavior between treated and untreated bronze samples, aligning with our objective of assessing the impact of surface treatments on corrosion resistance [80]. Moreover, the potentiostatic results provide valuable insights into the durability of the passive film under corrosive conditions. The increasing passivation current density observed, even in the presence of surface treatments, suggests potential breakdown of the passive layer or the influence of specific environmental factors. Connecting these potentiostatic results to our broader research objectives, we can assert that the observed variations in passive film behavior directly impact bronze corrosion susceptibility. The effectiveness of surface treatments in influencing these outcomes underscores the potential for tailored treatments to enhance overall bronze corrosion resistance. The potentiostatic results serve as a critical link in achieving our study objectives by shedding light on passive film behavior under different conditions, contributing to a more comprehensive understanding of corrosion mechanisms and emphasizing the significance of surface treatments in preserving bronze artifacts [81].

The data provided in Table 4 offers electrochemical parameters and inhibition efficiency values for bronze exposed to a 3.5% NaCl solution with different inhibitors (2% Paraloid® 48 or 2% Paraloid® 66), both with and without the inclusion of ZnO nanoparticles. These parameters are essential for evaluating the effectiveness of these inhibitors in safeguarding bronze against corrosion in saline environments. The corrosion potential (Ecorr) signifies the electrode potential at which corrosion initiates, measured in volts (V) vs. Ag/AgCl reference electrode. In all instances, the inhibitors (2% P-48, 2% P-66) shift the Ecorr values to more negative potentials compared to the absence of inhibitors (blank), indicating a hindrance to the corrosion process. The introduction of ZnO nanoparticles further exacerbates this shift, suggesting enhanced protection. Ba and Bc denote the anodic and cathodic Tafel slopes, respectively, indicating the electrochemical reaction rates during corrosion. Smaller Ba and Bc values imply slower corrosion rates. In most cases, the inhibitors (2% P-48, 2% P-66) lead to reduced Ba and Bc values compared to the blank, indicating decreased corrosion rates. Incorporating ZnO nanoparticles alongside the inhibitors further diminishes these values, indicating enhanced inhibition. Icorr represents the corrosion rate, with lower values indicating slower corrosion rates. In all scenarios, the inhibitors decrease the Icorr values compared to the blank, signifying effective corrosion rate reduction. The addition of ZnO nanoparticles results in even lower Icorr values, demonstrating improved corrosion inhibition. RP gauges the material's resistance to corrosion, with higher values denoting better corrosion protection. The presence of inhibitors heightens RP values compared to the blank, indicating improved corrosion resistance. The addition of ZnO nanoparticles further elevates RP values, highlighting enhanced protection. Corrosion rate quantifies the material lost due to corrosion over a specific time. In all cases, the inhibitors reduce the corrosion rate compared to the blank. The addition of ZnO nanoparticles leads to even lower corrosion rates, underscoring the efficacy of the inhibitors in preserving bronze. Inhibition efficiency is a crucial parameter quantifying the effectiveness of inhibitors in thwarting corrosion. It's calculated by comparing the corrosion rate of the inhibited system to that of the blank and expressed as a percentage. The inhibition efficiency values indicate that both 2% Paraloid® 48 and 2% Paraloid® 66 are effective inhibitors, with inhibition efficiencies around 90%. However, with the addition of ZnO nanoparticles to these inhibitors, inhibition efficiency significantly rises to approximately 94%, indicating superior corrosion protection. In summary, the electrochemical parameters and inhibition efficiency data in Table 4 demonstrate that the presence of inhibitors (2% Paraloid® 48 or 2% Paraloid® 66) effectively reduces the corrosion rate of bronze in a 3.5% NaCl solution. Moreover, the inclusion of ZnO nanoparticles enhances the inhibitory properties of these inhibitors,

Table 4 Electrochemical parameters and inhibition efficiency for bronze in 3.5% NaCl containing different 2% Paraloid® 48 and 2% Paraloid® 66 without and with ZnO

Inhibitor Mix. Conc., (ppm)	E_{corr} (V) vs. Ag/AgCl	B_a (Vdec^{-1})	B_c (Vdec^{-1})	I_{corr} (A.cm^{-2})	R_P (Ohm.cm^2)	Corr. Rate, (mm/y)	Inhibition efficiency, (%)
Blank	-0.168 ± 0.005	0.609 ± 0.010	0.989 ± 0.015	$2.871e-4 \pm 0.005$	498 ± 10	2.76 ± 0.005	–
2% P-48	-0.204 ± 0.006	0.872 ± 0.012	0.297 ± 0.020	$0.920e-4 \pm 0.007$	752 ± 15	0.27 ± 0.03	90.21 ± 1.5
2% P-48+ZnO	-0.233 ± 0.008	0.951 ± 0.015	0.235 ± 0.018	$0.667e-4 \pm 0.006$	857 ± 20	0.16 ± 0.02	94.20 ± 1.8
2% P-66	-0.175 ± 0.004	0.726 ± 0.008	0.367 ± 0.012	$0.812e-5 \pm 0.003$	672 ± 12	0.29 ± 0.04	89.49 ± 1.2
2% P-66+ZnO	-0.192 ± 0.007	0.818 ± 0.010	0.296 ± 0.015	$0.718e-5 \pm 0.004$	786 ± 18	0.18 ± 0.02	93.47 ± 1.6

Fig. 10 Potentiostatic current transient curves produced by the bronze electrode at 0.0 V (Ag/AgCl) of the passive region in the absence (3.5% NaCl solution) and in the presence of **A** 2% Paraloid® 48 and/or ZnO nanoparticles + 2% Paraloid® 48 **B** Paraloid® 66 and/or ZnO nanoparticles + 2% Paraloid® 66
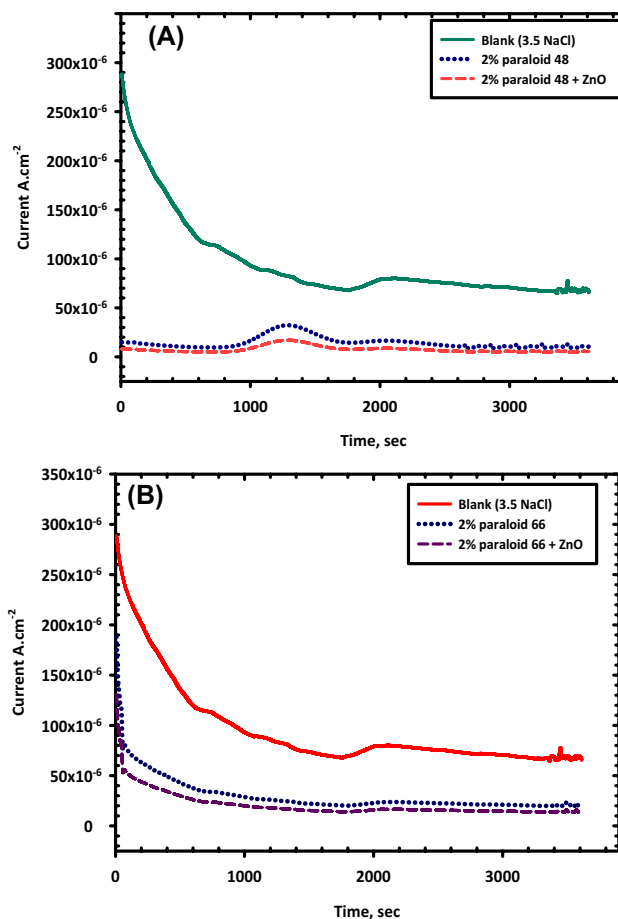
providing even better corrosion protection. These findings are instrumental in corrosion prevention strategies, particularly for preserving bronze artifacts in saline environments.

3.3 Current transients technique

Potentiostatic current transients are a common method for investigating the electrochemical characteristics of materials in various environments. These curves offer insights into the kinetics of electrochemical processes transpiring on the material's surface [82]. Here, we focus on the potentiostatic current transient curves generated by a bronze electrode at 0.0 V (Ag/AgCl) with and without the presence of Paraloid® 48, Paraloid® 66, and ZnO nanoparticles [83]. In the absence of additives, the potentiostatic current transient curve of the bronze electrode in a 3.5% NaCl solution typically exhibits a passive region, characterized by low current density, indicating minimal electrochemical activity [84]. When Paraloid® 48 and/or ZnO nanoparticles + 2% Paraloid® 48 are introduced, alterations in the passive region may occur, suggesting changes in the bronze electrode's surface and electrochemical behavior [85]. These modifications could arise from the adsorption of additives onto the electrode surface, influencing surface chemistry and electrochemical reactions (see Fig. 10a,b) [86]. Likewise, the presence of Paraloid® 66 and/or ZnO nanoparticles + 2% Paraloid® 66 may induce shifts in the potentiostatic current transient curve of the bronze electrode. Once again, these changes may stem from variations in surface chemistry prompted by the adsorption of additives [87]. In summary, the potentiostatic current transient curves of the bronze electrode, with and without Paraloid® 48, Paraloid® 66, and ZnO nanoparticles, may exhibit modifications in the passive region. These alterations likely result from shifts in surface chemistry due to additive adsorption. Further research is necessary to fully comprehend the mechanisms behind these changes and their implications for the electrochemical behavior of the bronze electrode [88].

3.3.1 Effect of sulfide injection on current transients of bronze

The effect of sulfide injection on the current transients of bronze electrodes in 3.5% NaCl in the presence of different inhibitors and nanoparticles can be discussed as follows.

3.3.1.1 2% paraloid® 48 and/or ZnO nanoparticles + 2% Paraloid® 48 In the presence of 2% Paraloid® 48 and/or ZnO nanoparticles + 2% Paraloid® 48, the bronze electrodes are expected to exhibit a lower corrosion rate compared to the uninhibited electrode see Fig. 11a. When the electrode is potentiostated at 0.0 V vs. Ag/AgCl for one hour in the inhibited electrolyte, a protective film is formed on the surface of the bronze electrode [89]. However, when 10^{-3} M sulfide ions are injected, the current transients of the bronze electrode are expected to increase due to the breakdown of the protective film. Sulfide ions can react with the metal cations in the protective film, leading to the formation of metal sulfides and subsequent detachment of the film. The extent of the current transient would depend on the concentration of sulfide ions and the thickness and quality of the protective film [90].

3.3.1.2 Paraloid® 66 and/or ZnO nanoparticles + 2% Paraloid® 66 Paraloid® 66 is a thermoplastic resin that has been reported to provide better corrosion protection compared to Paraloid® 48. ZnO nanoparticles, when used in combination with Paraloid® 66, can further enhance the corrosion resistance of the metal surface [91]. Like the case of 2% Paraloid® 48 and/or ZnO nanoparticles + 2% Paraloid® 48, the bronze electrodes in the presence of Paraloid® 66 and/or ZnO nanoparticles + 2% Paraloid® 66 are expected to exhibit a lower corrosion rate. When the electrode is potentiostated at 0 V vs Ag/AgCl for one hour in the inhibited electrolyte, a protective film is formed on the surface of the bronze electrode see Fig. 11b. However, when 10^{-3} M sulfide ions are injected, the current transients of the bronze electrode are expected to increase due to the breakdown of the protective film [92]. The extent of the current transient would depend on the con-

Fig. 11 Effect of sulfide injection on the current transients of bronze electrodes in 3.5% NaCl in the presence of **A** 2% Paraloid® 48 and/or ZnO nanoparticles + 2% Paraloid® 48 **B** Paraloid® 66 and/or ZnO nanoparticles + 2% Paraloid® 66
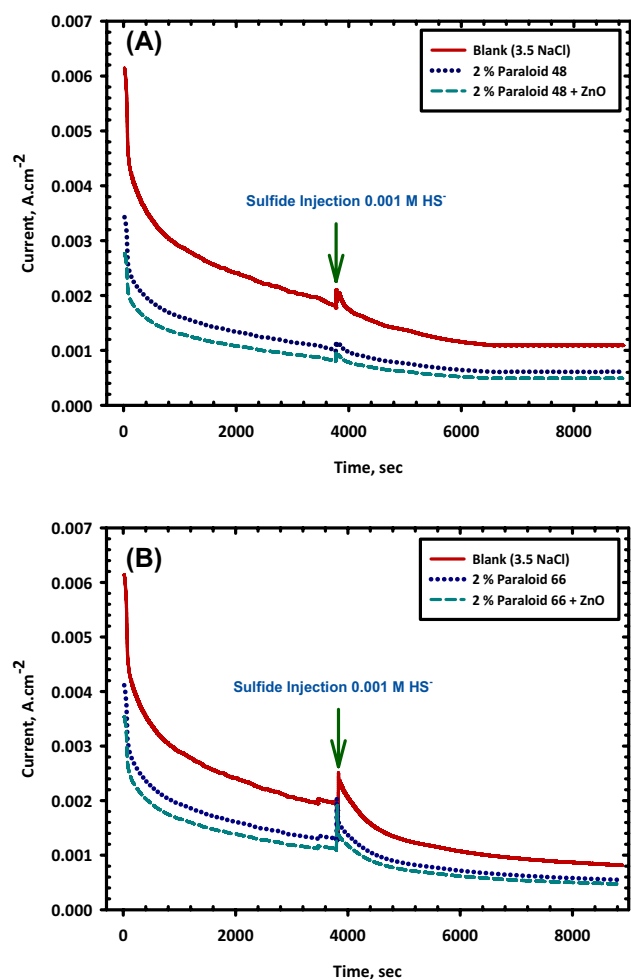
centration of sulfide ions and the thickness and quality of the protective film [93]. Overall, the injection of sulfide ions is expected to lead to an increase in the current transients of the bronze electrodes, regardless of the type of inhibitor and nanoparticle used. However, the extent of the increase would depend on several factors, including the concentration of sulfide ions, the type and concentration of the inhibitor and nanoparticle, and the quality of the protective film formed on the surface of the electrode [94].

3.4 Electrochemical impedance spectroscopy

Figure 12 offers a detailed visualization of Electrochemical Impedance Spectroscopy (EIS) outcomes, focusing on the influence of ZnO nanoparticles on bronze corrosion within a 3.5% NaCl solution with 2% Paraloid® 48 or Paraloid® 66 coatings. The figure is divided into several subplots, each providing unique insights into the electrochemical behavior. Subplots A and B depict Nyquist plots, showcasing impedance data from EIS analysis. These plots compare conditions with and without ZnO nanoparticles, revealing potential changes in corrosion resistance. Variations in impedance values and plot shapes indicate alterations in electrochemical properties. Subplots C and D present Bode plots derived from EIS data, offering a frequency response overview. Changes in impedance magnitude and phase angle across frequencies reflect the impact of ZnO nanoparticles on system behavior and coating efficacy. Subplot E presents an equivalent circuit model representing the electrochemical system. This model aids in interpreting complex electrochemical responses observed in experiments. The inclusion of ZnO nanoparticles with Paraloid® coatings may modify circuit parameters, reflecting changes in system behavior. Overall, Fig. 12 provides a comprehensive understanding of how ZnO nanoparticles influence bronze corrosion in specific conditions. Insights into impedance changes, electrochemical responses, and coating effectiveness are crucial for grasping the mechanisms behind nanoparticle-induced corrosion control. Furthermore, assessing the goodness of fit between experimental data and the circuit model is essential for method credibility. Chi-squared values, calculated for EIS measurements, indicate the agreement between the applied model and experimental results. A low chi-squared value, close to 1, demonstrates a good fit, ensuring the reliability of data interpretation. The use of Gamry Echem Analyst™ for data fitting enhances accuracy and transparency in electrochemical parameter extraction. Moreover, discussing the Warburg element's role in EIS results provides valuable insights into diffusion processes at the electrode–electrolyte interface. The presence of the Warburg element in the equivalent circuit model elucidates diffusion-controlled phenomena, particularly relevant for systems with passive films. Its characteristics, such as frequency-dependent impedance, offer information about ion transport kinetics and passive film behavior, enriching the understanding of corrosion resistance mechanisms. In summary, Fig. 12 and the discussion of chi-squared values and the Warburg element contribute significantly to the comprehensive analysis of bronze corrosion behavior and highlight the importance of considering both electrochemical and diffusional aspects in corrosion studies.

Table 5 showcases electrochemical impedance parameters and inhibition efficiency values for bronze immersed in a 3.5% NaCl solution with and without different inhibitors (2% Paraloid® 48 or 2% Paraloid® 66), along with ZnO nanoparticles. Electrochemical impedance spectroscopy (EIS) is instrumental in assessing corrosion resistance and inhibitor effectiveness. Rs denotes electrolyte solution resistance, influenced by solution conductivity. Inhibitors and ZnO nanoparticles slightly raise Rs values, indicating minor impact on solution resistance. Cb represents double-layer capacitance, reflecting charge separation at the metal-electrolyte interface. Reduced Cb values with inhibitors suggest a more stable double layer. Rb, indicating charge transfer resistance, increases with inhibitors, indicating slower corrosion rates. Addition of ZnO nanoparticles further boosts Rb, emphasizing enhanced corrosion protection. W, associated with diffusion processes, decreases with inhibitors and ZnO nanoparticles, indicating improved mass transport. Inhibition efficiency (I.E) quantifies inhibitor effectiveness, comparing impedance parameters of inhibited and uninhibited systems. Both Paraloid® 48 and Paraloid® 66 exhibit inhibition efficiencies of approximately 87–89%, while inclusion of ZnO nanoparticles increases I.E to around 91–94%, indicating superior corrosion protection. In summary, electrochemical impedance parameters demonstrate that inhibitors enhance bronze corrosion resistance, with ZnO nanoparticles further amplifying protection. These findings are crucial for corrosion prevention, particularly in safeguarding bronze artifacts in saline environments. Discussing the Constant Phase Element (CPE) enriches understanding of system electrical behavior in EIS analysis. The CPE in the equivalent circuit model accommodates non-ideal behavior, such as heterogeneities or surface irregularities. Observed as a depressed semicircle in Nyquist plots, CPE introduces a frequency-dependent phase shift, with its exponent 'n' indicating the nature of non-ideal behavior. The CPE's relevance lies in capturing complexities of the bronze-electrolyte interface, contributing to nuanced interpretation of impedance data. Its inclusion enhances fidelity in modeling non-ideal behavior, offering insights into passive film complexities and corrosion mechanisms affecting bronze samples.
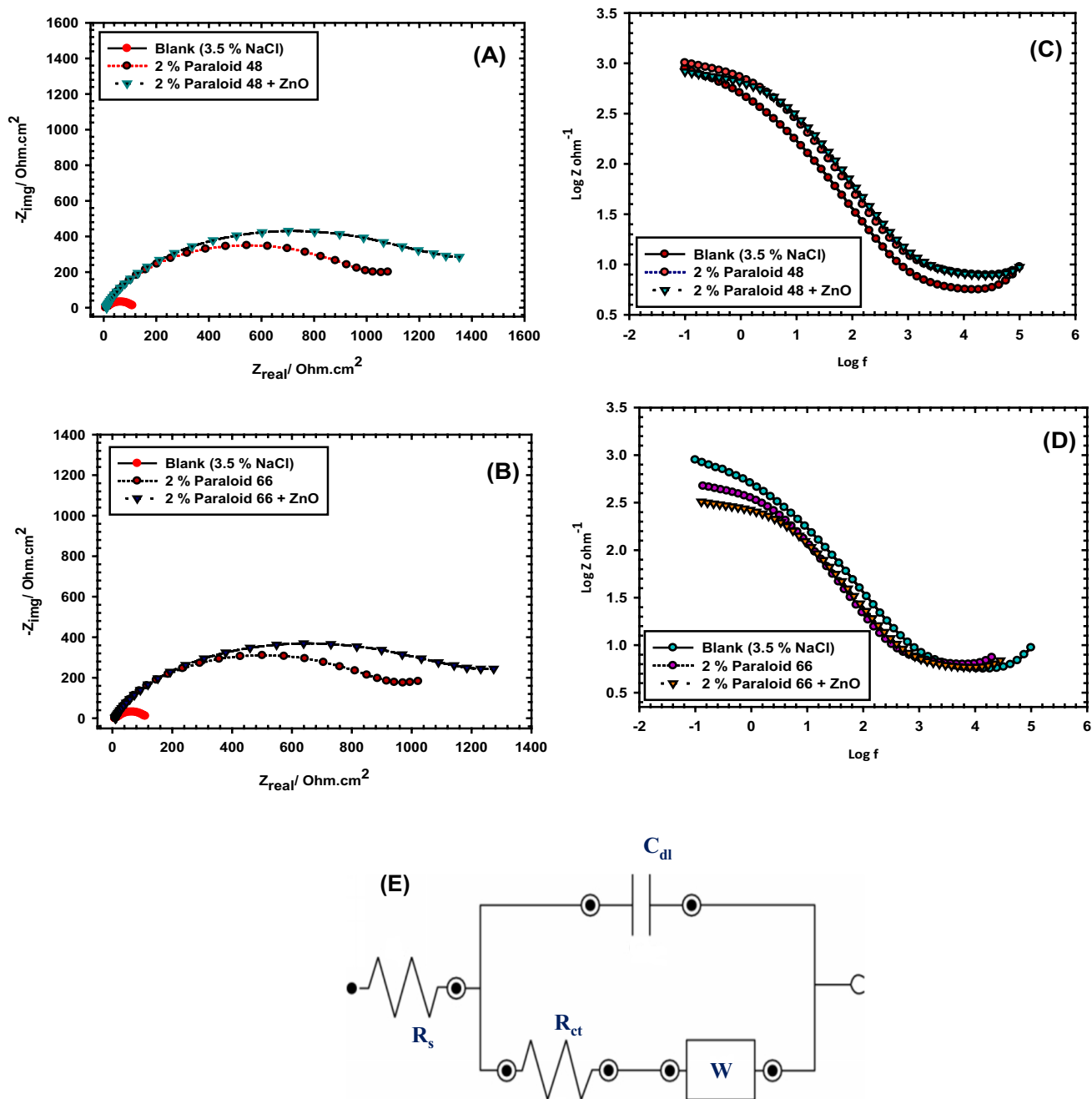
Fig. 12 Represent the EIS Figures for the effect of adding ZnO nanoparticles on the corrosion behavior of bronze in 3.5% NaCl solution containing, 2% Paraloid® 48 and Paraloid® 66, **A** and **B** Nyquist plots. **C** and **D** Bode plots. **E** Equivalent circuit

Table 5 Electrochemical Impedance parameters and inhibition efficiency for bronze in 3.5% NaCl containing different 2% Paraloid® 48 and 2% Paraloid® 66 without and with ZnO

Inhibitor conc., (ppm)	R_s (Ohm.cm^2)	C_p (micro Fcm^{-2})	R_p (Ohm.cm^2)	W (micro-Mho)	I.E (%)
Blank	7.87 ± 0.15	199.6 ± 3.5	52 ± 1.2	33.9 ± 0.7	–
2% P-48	9.17 ± 0.20	45.48 ± 1.0	538 ± 10	3.7 ± 0.1	89.08 ± 1.3
2% P-48 + ZnO	9.58 ± 0.25	37.81 ± 0.8	598 ± 12	2.1 ± 0.05	93.80 ± 1.6
2% P-66	8.98 ± 0.18	41.13 ± 0.9	474 ± 8	4.1 ± 0.2	87.90 ± 1.4
2% P-66 + ZnO	9.34 ± 0.22	36.26 ± 0.7	523 ± 9	2.8 ± 0.15	91.74 ± 1.5

The given statement describes the effect of immersion time on the sudden decrease of R_p (polarization resistance) upon injection of 10^{-3} M sulfide ions, as determined by the electrochemical impedance spectroscopy (EIS) technique, of a bronze electrode immersed in a solution of 3.5% NaCl and either 2% Paraloid® 48 and/or ZnO nanoparticles + 2% Paraloid® 48 or Paraloid® 66 and/or ZnO nanoparticles + 2% Paraloid® 66 [95]. The polarization resistance (R_p) is a measure of the resistance to the flow of current through an electrochemical system see Fig. 13a, b. The sudden decrease in R_p upon injection of sulfide ions suggests that the bronze electrode is undergoing a corrosion process, as sulfide ions are known to be aggressive towards metals. Immersion time refers to the duration for which the bronze electrode is exposed to the corrosive solution [96]. As the immersion time increases, the corrosion rate is expected to increase due to the accumulation of corrosion products and the continuous supply of corrosive species [97]. The effect of immersion time on the sudden decrease of R_p may differ between the two systems (Fig. 13a, b) due to the difference in the types of nanoparticles used (Paraloid® 48 and Paraloid® 66) and their concentration. Paraloid® 48 and Paraloid® 66 are both types of polymers that are used as binders, while ZnO nanoparticles are known for their corrosion-inhibiting properties. In Fig. 13 a, the addition of ZnO nanoparticles and Paraloid® 48 may have a synergistic effect on reducing the corrosion rate of the bronze electrode. The Paraloid® 48 may act as a barrier to prevent the access of sulfide ions to the bronze surface, while the ZnO nanoparticles may act as a sacrificial anode to reduce the corrosion rate by undergoing corrosion themselves. In Fig. 13b, the addition of Paraloid® 66 may not have a significant effect on reducing the corrosion rate, as it is not known for its barrier properties. However, the addition of ZnO nanoparticles may still provide some level of corrosion protection. Overall, the effect of immersion time on the sudden decrease of R_p may depend on various factors such as the composition and concentration of the corrosive solution, the type and concentration of nanoparticles used, and the type of metal being studied. Further experiments and analysis are needed to fully understand the effect of immersion time on the corrosion behavior of the bronze electrode in these systems [98].

Fig. 13 Effect of immersion time on the sudden decrease of R_p upon injection of 10^{-3} M sulfide ions of polarization resistance, determined by EIS technique, of a bronze electrode immersed in a solution of 3.5% NaCl and **A** 2% Paraloid® 48 and/or ZnO nanoparticles + 2% Paraloid® 48. **B** Paraloid® 66 and/or ZnO nanoparticles + 2% Paraloid® 66
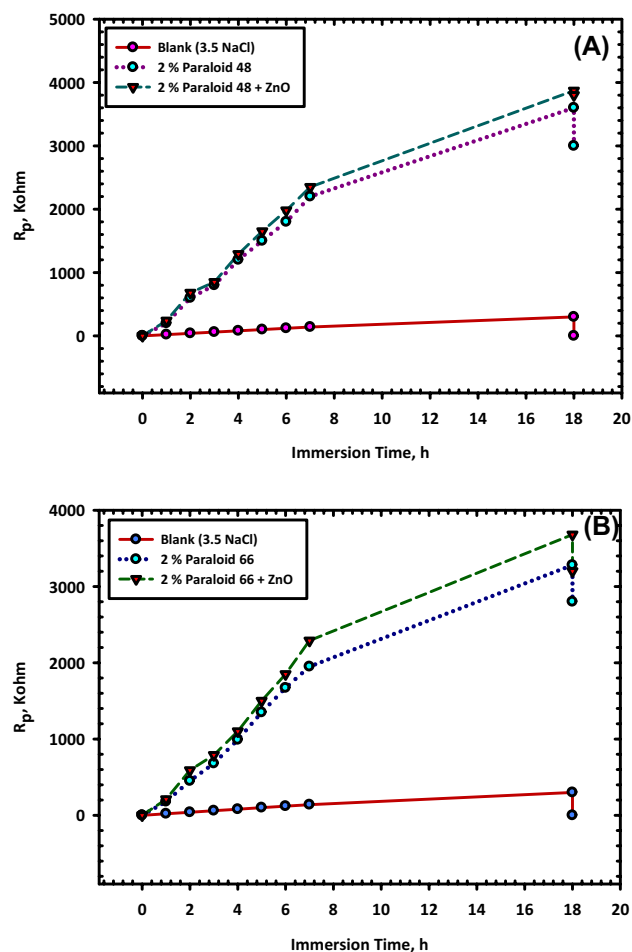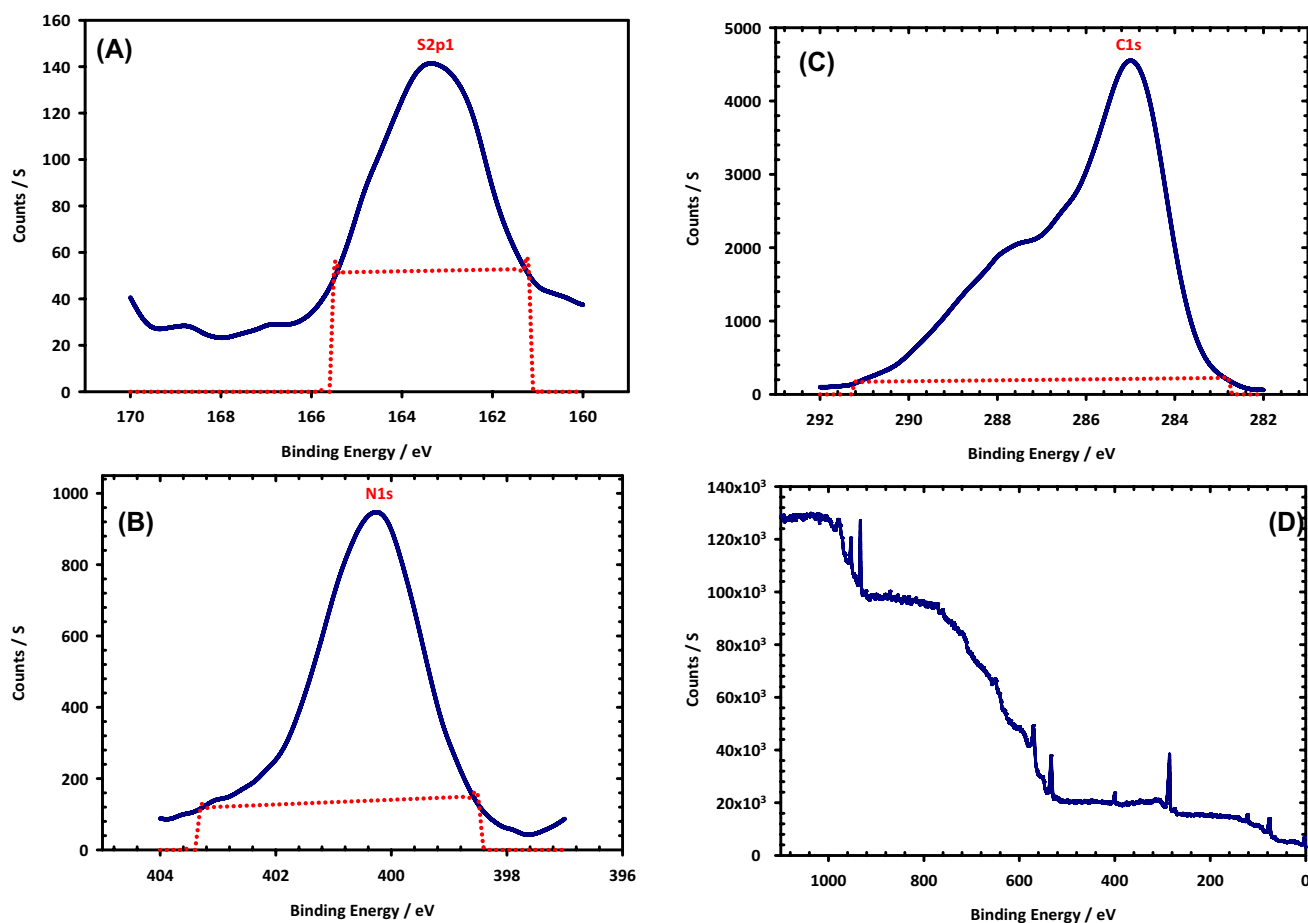
Fig. 14 Displays various segments of the XPS spectra of copper that was submerged in a solution of 3.5% NaCl and 10–2 M BTAH. After 17 h, 10^{-3} M HS⁻ was added to the solution, and the electrode stayed in touch with the solution for one hour following the addition of sulphide. **A** represents the sulfide on the bronze electrode, **B** represents the nitrogen content, **C** represents the carbon content and **D** represents the survey on the surface of the sample

3.5 X-ray photoelectron spectroscopy (XPS)

The chemical composition of the surface of bronze arrowheads before and after being attacked by sulfides may be studied by X-ray photoelectron spectroscopy (XPS). The X-ray photoelectron spectrometer (XPS) determines the elements and chemical states of a sample by measuring the binding energy of electrons released from its surface upon X-ray irradiation [99]. The XPS spectrum of bronze arrowheads before the sulfide attack would exhibit peaks at the energies of the elements present in the bronze alloy, including copper and tin. Depending on the bronze alloy's exact makeup, the relative strengths of these peaks will vary. A post-sulfide assault XPS spectra of the arrowheads' surfaces would most likely exhibit new peaks attributable to the presence of sulfite molecules. Sulfur and copper sulfide peaks, to name two examples, might be present. The severity and length of the sulfide assault would determine the strength of these peaks and the level of surface sulfurization. To further comprehend the chemical events taking place during the sulfide assault, XPS may also reveal the oxidation state of the components present on the arrowheads' surfaces. A possible indicator that the copper on the arrowheads' surfaces was oxidized by the sulfide assault is the presence of copper in its oxidized form (Cu^{2+}) rather than its metallic state (Cu^{0}). Some of the XPS spectra measured from a corroded copper surface are shown in Fig. 14. The electrode was exposed to 10–2 M BTAH at 0 V against Ag/AgCl for 17 h, following which 10–3 M HS- was injected and stayed in contact with the copper surface for 1 h. According to the XPS spectra, the N1s peak has a binding energy of 400 eV, the $S^{2}p$ peak has a binding energy of 162.0 eV, and the C1s peak has a binding energy of 284.6 eV. This proves that BTAH coexisted with sulfide ions on the corroded copper surface. The $S^{2}p$ signal at 162.0 eV also indicates the existence of sulfide ions, which is consistent with copper sulfide. Due to the lack of an $S^{2}p$ signal at 164.0 eV, we

may conclude that elemental sulfur was not present on the corroded copper surface [100]. This lends credence to the hypothesis that copper dissolution owing to sulfide ions is responsible for the increased current seen in Figs. 2 and 4, 5, 6 and 7, rather than sulfide ion oxidation.

3.6 Treatment and conservation of arrowheads

The arrowheads underwent chemical treatment followed by meticulous manual cleaning to reveal their natural surface pattern. Despite being in excellent metallic condition, they were covered with extensive corrosion products. Through a series of trials, various chemical compounds were tested to find the most effective solution for dissolving corrosion layers while minimizing damage to the arrowheads [101]. Different concentrations and treatment durations were employed for each compound. The chosen method involved submerging the arrowheads in an alkaline Rochelle solution containing sodium hydroxide and sodium potassium tartrate to dissolve copper II compounds in the corrosion layers. A soft silk brush was used along with multiple changes of cleaning solution to aid in the process. While the green copper corrosion products were successfully removed, a reddish-brown covering remained on the anklet surfaces. The oxide layer (cuprite) was dissolved using a 2% sulfuric acid solution and then brushed away [102]. This process was repeated until all traces of corrosion vanished. Submerging the objects in water and scrubbing them with a toothbrush helped remove any residue from tiny crevices. Afterwards, the arrowheads were washed in hot, deionized water to flush out any remaining chemical residue, utilizing cycles of heating and cooling. They were then dried using ether and hot sawdust before being patted dry with a soft, clean towel. Finally, they were disentangled using a technique depicted in Fig. 15a–d. In summary, the corrosion coatings on the arrowheads were dissolved and removed through a combination of chemical and mechanical treatments, restoring their original metallic state. This involved applying specific chemical substances for varying durations, followed by thorough washing and drying, ultimately revealing the arrowheads' original surface topography. Subsequently, the arrowheads were treated with ZnO nanoparticles in combination with Paraloid® 48 before being handed over to the Military Museum organization, Al-Qala, Cairo, Egypt. Providing detailed information on treatment duration, specific procedures, ZnO and Paraloid® concentrations, electrolyte preparation, and post-treatment procedures is essential for transparency and reproducibility [103]. These surface treatments aim to enhance the corrosion resistance of bronze samples, and the subsequent electrochemical measurements evaluate their effectiveness in achieving this goal.

3.7 Mode of action

Metallographic examinations (ME) of the arrowheads revealed elongated bronze grains, indicating the use of a hammering method during manufacturing post-casting [104]. However, this method introduced strains within the metallic structure, leading to deterioration. The metal surface exhibited uniform corrosion spots, pitting corrosion, and micro-cracks, distorting the surface of all objects [105]. Micro-cracks were distributed widely, resulting from high stresses endured during forming, usage, or burial [106]. Scanning electron microscopy confirmed the presence of various forms of corrosion, including pitting, stress corrosion, and crevice corrosion, across the alloy. Several objects were made of tin bronze, an alloy of copper and another metal, with a tin percentage typically between 7.83% and 9.90% [107]. Historical accounts suggest that tin could enrich the surface as a semi-transparent tin oxide coating, while copper was depleted. The uneven composition made the bronze vulnerable to selective corrosion by corrosive chemicals [108]. However, the alpha phase's structural formation endowed it with desirable mechanical qualities such as high tensile strength and hardness [109]. X-ray diffraction analysis identified corrosion products including cuprite, quartz, brochantite, paratacamite, malachite, and antlerite. Sulfide corrosion occurred during the artifacts' time at the military museum, evidenced by the presence of brochantite and antlerite [110]. Paraloid® resin, often used in conservation treatments, has been enhanced with nano-composites to improve its performance in preserving bronze artifacts. Studies show that Paraloid® nanocomposites offer protection against environmental variables and can build a sturdy protective coating, increasing durability [111]. Nano-composites were tested on bronze sculptures and copper coins, reducing corrosion and enhancing longevity without altering visual appeal [112]. Zinc oxide nanoparticles (ZnO) have been researched for use in preserving cultural heritage artifacts like bronze sculptures. Adding nano ZnO to Paraloid® improves its performance as a consolidant, enhancing hardness, tensile strength, and resilience to environmental variables [113]. The antibacterial properties of nano ZnO may inhibit microbe growth on bronze objects, crucial for damp storage conditions. Removing disfiguring corrosion from metals often requires chemical treatments when mechanical cleaning is impractical due to thick, hard layers combined with soil debris [114]. X-ray fluorescence (XRF) has been utilized to identify alloys in historical bronze artifacts without causing damage [115]. In conclusion, preserving bronze artifacts requires a multifaceted approach involving chemical

Fig. 15: a, **b**, **c**, **d** Show the arrowheads after treatment
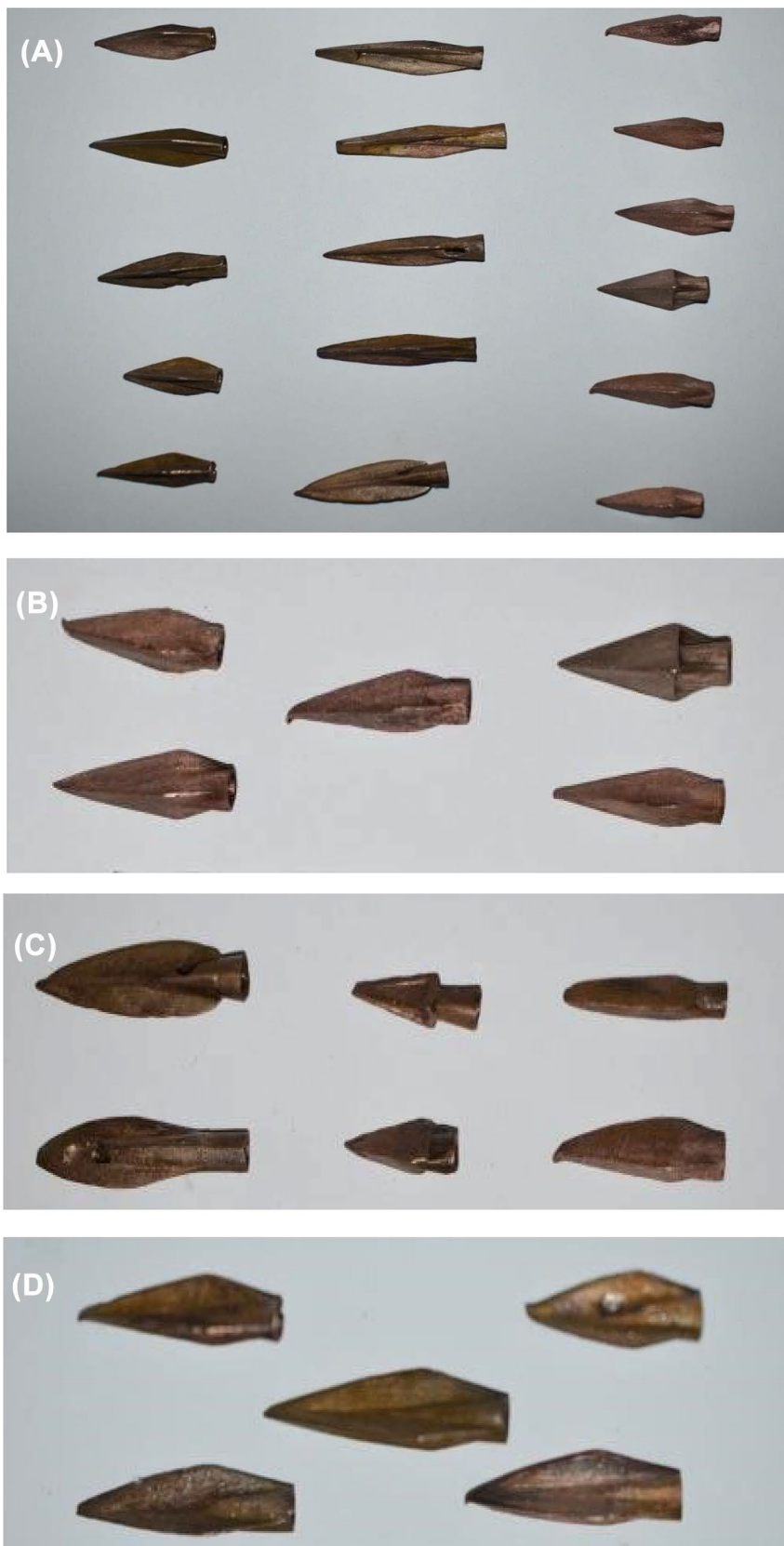
treatments, enhanced resin coatings, and nanoparticle additives to combat corrosion and degradation effectively while preserving the objects' integrity [116–118].

4 Conclusion

Examinations and analyses revealed widespread pitting corrosion and micro-cracks on the objects' surfaces. XRD analysis identified various corrosion products, indicating a significant interaction between the objects and their environment. Cleaning methods depend on factors like the object's condition and desired outcome, with modern equipment aiding informed decisions. Both 2% Paraloid® 48 and/or ZnO nanoparticles + 2% Paraloid® 48, and Paraloid® 66 and/or ZnO nanoparticles + 2% Paraloid® 66 offer effective corrosion protection for bronze electrodes in a 3.5% NaCl solution. Adding ZnO nanoparticles enhances their protective capabilities by creating a physical barrier, reducing contact with the corrosive solution. The choice between options may consider cost, availability, and specific application requirements. Regular maintenance and inspection remain necessary for continued protection. Inhibition efficiency results from PD indicate promising outcomes for corrosion mitigation. 2% P-48 alone exhibited significant inhibition efficiency (90.21%), highlighting its inherent corrosion-inhibiting properties. Incorporating ZnO into the mixtures enhanced inhibition efficiency, with combinations of 2% P-48 with ZnO reaching 94.20%, and 2% P-66 with ZnO reaching 93.47%. ZnO demonstrates potential as a synergistic corrosion inhibitor, augmenting the effectiveness of P-48 and P-66. The mixtures, especially with ZnO, show higher inhibition efficiency, suggesting tailored combinations for optimized corrosion protection. These results offer insights into effective corrosion inhibition strategies, with ZnO showing promise for tailored combinations to enhance protection in specific environments.

Data availability All data generated or analyzed during this study are included in this published article.

Declarations

Competing interests The authors declare that there is no conflict of interest. On behalf of all authors, the corresponding author states that there is no conflict of interest.

References

1. Abdelshafeek KA, El-Shamy AM. Review on glucosinolates: unveiling their potential applications as drug discovery leads in extraction, isolation, biosynthesis, biological activity, and corrosion protection. Food Biosci. 2023;56: 103071. https://doi.org/10.1016/j.fbio.2023.103071.
2. El-Shamy AM, Mouneir SM. Medicinal materials as eco-friendly corrosion inhibitors for industrial applications: a review. J Bio Tribo-Corros. 2023;9(1):3. https://doi.org/10.1007/s40735-022-00714-9.
3. Kiele E, Senvaitiene J, Griguceviciene A, Ramanauskas R, Raudonis R, Kareiva A. Application of the sol-gel method for the conservation of copper alloys. Micro Chem J. 2016;124:623–8.
4. Mohamed OA, Farghali AA, Eessaa AK, El-Shamy AM. Cost-effective and green additives of pozzolanic material derived from the waste of alum sludge for successful replacement of Portland cement. Sci Rep. 2022;12:20974. https://doi.org/10.1038/s41598-022-25246-7.
5. Muller J, Laïk B, Guillot I. α-Cu Sn bronzes in sulfate medium: Influence of the tin content on corrosion processes. Corros Sci. 2013;77:46–51.

6. Robbiola L, Blengino M, Fiaud C. Morphology, and mechanisms of formation of natural patinas on archaeological Cu–Sn alloys. Corros Sci. 1998;40(12):2083–111.
7. Abdelshafeek KA, Abdallah WE, Elsayed WM, Eladawy HA, El-Shamy AM. Vicia faba peel extracts bearing fatty acids moieties as a cost-effective and green corrosion inhibitor for mild steel in marine water: computational and electrochemical studies. Sci Rep. 2022;12(1):20611. https://doi.org/10.1038/s41598-022-24793-3.
8. Casaletto MP, Vilma B. Sustainable conservation of bronze artworks: advanced research in materials science, in XIXth International Congress on Ancient Bronzes, Getty Conservation Institute, Los Angeles. 2017.
9. Zohdy KM, El-Sherif RM, El-Shamy AM. Effect of pH fluctuations on the biodegradability of nanocomposite Mg-alloy in simulated bodily fluids. Chem Paper. 2022;2022:1–21. https://doi.org/10.1007/s11696-022-02544-y.
10. Hamidah I, Solehudin A, Hamdani A, Hasanah L, Khairurrijal K, Kurniawan T, Hammouti B. Corrosion of copper alloys in KOH, NaOH, NaCl, and HCl electrolyte solutions and its impact to the mechanical properties. Alex Eng J. 2021;60(2):2235–43.
11. Borgia G, Iacobucci G, Pelosi C, Romani A, Stazi MA. Characterization of corrosion products on bronze artifacts, and the development of conservation treatments. Stud Conserv. 2017;62(4):209–17.
12. Casaletto MP, Cirrincione C, Privitera A, Basilissi V, (2016) A sustainable approach to the conservation of bronze artworks by smart nanostructured coatings. In Proceedings of Metal 2016, 9th interim meeting of the ICOM-CC Metals Working Group, New Delhi, 26–30 September.
13. Mouneir SM, El-Hagrassi AM, El-Shamy AM. A review on the chemical compositions of natural products and their role in setting current trends and future goals. Egypt J Chem. 2022;65(5):491–506. https://doi.org/10.21608/ejchem.2021.95577.4486.
14. Ghazy EA, Abdel GN, A., El-Shamy A. M.,. Comparative study of cetyl trimethyl ammonium bromide, formaldehyde, and isobutanol against corrosion and microbial corrosion of mild steel in chloride media. J Bio Tribo-Corros. 2023;9:64. https://doi.org/10.1007/s40735-023-00782-5.
15. Megahed MM, Abdel Bar MM, Abouelez ESM, El-Shamy AM. Polyamide coating as a potential protective layer against corrosion of iron artifacts. Egypt J Chem. 2021;64(10):5693–702. https://doi.org/10.21608/ejchem.2021.70550.3555.
16. Boccia PA. The formation of acetate corrosion on bronze antiquities: characterization and conservation, Doctoral dissertation, University College, London. 2011; 213.
17. Megahed MM, Youssif M, El-Shamy AM. Selective formula as a corrosion inhibitor to protect the surfaces of antiquities made of leather-composite brass alloy. Egypt J Chem. 2020;63(12):5269–87. https://doi.org/10.21608/ejchem.2020.41575.2841.
18. Fjaestad M, et al. The decay of archaeological copper alloy artifacts in soil, in Metal 95. London: James LTD; 1997.
19. El-Shamy AM. Cathodic Protection in the oil and gas industries, in corrosion and materials in the oil and gas industry. 2016; 489–510.
20. Mahmoud G. Corrosion Characteristics and conservation of ancient Egyptian bronze osiris statuette from Al-Arish museum. Egyp J Archaeol Restoration Stud. 2022;12(1):65–71.
21. Reda Y, El-Shamy AM, Eessaa AK. Effect of hydrogen embrittlement on the microstructures of electroplated steel alloy 4130. Ain Shams Eng J. 2018;9(4):2973–82. https://doi.org/10.1016/j.asej.2018.08.004.
22. Elashery NH, Megahed MM, El-Shamy AM, Saleh SM. Archaeometric characterization and conservation of bronze patina on archaeological axe head in military museum, Cairo. J Archaeol Tour Must. 2023;2(1):23–33.
23. Alwaleed RA, Megahed MM, Elamary RB, El-Shamy AM, Ali YS. Remediation mechanism of microbial corrosion for iron artifacts buried in soil by using allium sativum (garlic extract) as a natural biocide. Egypt J Chem. 2023;66(6):291–308.
24. Reda Y, Yehia HM, El-Shamy AM. Triple aging of the RRA Al-Cu 2024 alloy and its impact on the mechanical and microstructure properties. Egypt J Pet. 2022;31:89–94. https://doi.org/10.1016/j.ejpe.2022.08.003.
25. Feretti MO, Miazzo L, Moioli,. The application of nondestructive XRF method to identify different alloys in the bronze statue of the Capitoline horse. Stud Conserv. 1997;42(4):241–6.
26. Scott DA. Bronze disease: a review of some chemical problems and the role of relative humidity. J Am Inst Conserv. 1990;29:193–206.
27. Correa MA, Fernández MJ, Damborenea JJ, Skeldon P. Conservation of bronze artifacts by electrochemical reduction. Electrochim Acta. 2018;283:112–21. https://doi.org/10.1016/j.electacta.2018.06.084.
28. Wang Q. An investigation of deterioration of archaeological iron. Stud Conserv J. 2007;52:125.
29. Madsen B. Mikrobiologsk angreb pa bronzerne Fra Budsenebronden. Meddelelser, om Konservering. 1977;2:264–70.
30. Blanes MD, Fernández MJ, Damborenea JJ, Skeldon P. Corrosion protection of bronze using hybrid organic-inorganic coatings. Prog Org Coat. 2019;130:135–45. https://doi.org/10.1016/j.porgcoat.2019.03.019.
31. Madsen B, Hansen H. Black spots on bronzes a microbiological chemical attack on bronzes, in the conservation and restoration of metals, Scottish Society for conservation and restoration, Edinburgh, 1979; 33-39
32. Abbas MA, Ismail AS, Zakaria K, El-Shamy AM, El-Abedin SZ. Adsorption, thermodynamic, and quantum chemical investigations of an ionic liquid that inhibits corrosion of carbon steel in chloride solutions. Sci Rep. 2022;12:12536. https://doi.org/10.1038/s41598-022-16755-6.
33. Madsen B, Hansen H. A note on black spots on bronzes, in science and technology in the service of conservation. London. 1982;27:125.
34. Elsayed EM, Eessaa AK, Abdelbasir SM, Rashad MM, El-Shamy AM. Fabrication, characterization, and monitoring the propagation of nanocrystalline ZnO thin film on ITO substrate using electrodeposition technique. Egypt J Chem. 2023;66(2):33–43. https://doi.org/10.21608/ejchem.2022.126134.5595.
35. Oddy WA, Meeks ND. Unusual phenomena in the conservation of ancient bronzes in science and technology in the service of conservation, London. 1989; 119–124.
36. Gad EA, El-Shamy AM. Mechanism of corrosion and microbial corrosion of 1,3-dibutyl thiourea using quantum chemical calculations. J Bio Tribo-Corros. 2022;8:71. https://doi.org/10.1007/s40735-022-00669-x.
37. Frant MS. Copper sulphide creeps on porous electroplate. J Electrochem Soc. 1960;107:1009–11.
38. Abdel-Karim AM, El-Shamy AM, Reda Y. Corrosion and stress corrosion resistance of Al Zn alloy 7075 by nano-polymeric coatings. J Bio Tribo-Corros. 2022;8:57. https://doi.org/10.1007/s40735-022-00656-2.
39. Kawawata S, Ogura J. Chemical tree deterioration in the insulations of plastics- insulated wires and cables. Hitch Rev. 1971;20:55–63.
40. Abdel-Karim AM, El-Shamy AM. A review on green corrosion inhibitors for protection of archeological metal artifacts. J Bio Tribo-Corros. 2022;8:35. https://doi.org/10.1007/s40735-022-00636-6.

41. Hansen NH. Cleaning and stabilization of sulfide corroded bronzes. Stud Conserv. 1984;29:17–20.
42. Reda Y, Yehia HM, El-Shamy AM. Microstructural and mechanical properties of Al-Zn alloy 7075 during RRA and triple aging. Egypt J Pet. 2022;31:9–13. https://doi.org/10.1016/j.ejpe.2021.12.001.
43. El-Shamy AM. Control of corrosion caused by sulfate-reducing bacteria. Microbes Process. 2014;31:337–62.
44. Ateya BG, Alkharafi FM, El-Shamy AM, Abdalla RM. Electrochemical oxidation of hydrogen sulfide in geothermal fluids under high temperature and pressure. In: ACS National Meeting Book of Abstracts 2008 236th National Meeting and Exposition of the American Chemical Society, ACS 200817 August (2008) through 21 August.
45. Ateya BG, Alkharafi FM, El-Shamy AM, Saad AY, Abdalla RM. Electrochemical desulphurization of geothermal fluids under high temperature and pressure. J Appl Electrochem. 2009;39:383–9. https://doi.org/10.1007/s10800-008-9683-3.
46. Scott D. Periodic corrosion phenomena in bronze antiquities. Stud Conserv. 1985;30:49–57.
47. Sandu I, Quaranta M, Bejinariu C, Sandu IG, Luca D, Sandu AV. Study on the specific effects of corrosion processes on ancient bronze artifacts, annals of "Dunărea de Jos" university of Galati Fasc IX. Metallur Mater Sci. 2007;1:64–63.
48. El-Shamy AM, Soror TY, El-Dahan HA, Ghazy EA, Eweas AF. Microbial corrosion inhibition of mild steel in salty water environment. Mater Chem Phys. 2009;114(1):156–9. https://doi.org/10.1016/j.matchemphys.2008.09.003.
49. Alkharafi FM, El-Shamy AM, Ateya BG. Comparative Effect of toly triazole and benzotriazole against sulfide attack on copper. Int J Electrochem Sci. 2009;4:1351–64.
50. Oddy WA, Meeks ND. Unusual phenomena in the corrosion of ancient bronzes, Science and technology in the service of conservation. In: Brommelle NS, Thomson G. (Eds). International Institute for Conservation of Historic and Artistic Works, London. 1982; 119–124.
51. Thickett D, Odlyha M. Note on the identification of an unusual pale blue corrosion product from Egyptian copper alloy artifacts. Stud Conserv. 2000;45(1):63–7.
52. Sherif EM, Abbas AT, Gopi D, El-Shamy AM. Corrosion and corrosion inhibition of high strength low alloy steel in 2.0 M sulfuric acid solutions by 3-amino-1,2,3-triazole as a corrosion inhibitor. J Chem. 2014. https://doi.org/10.1155/2014/538794.
53. El-Shamy AM, Shehata MF, Ismail AIM. Effect of moisture contents of bentonitic clay on the corrosion behavior of steel pipelines. J Appl Clay Sci. 2015;114:461–6. https://doi.org/10.1016/j.clay.2015.06.041.
54. Trentelman K, Stodulski L, Scott D, Back M, Stock S, Strahan D, Drews AR, O'Neill A, Weber WH, Chen AE, Garrett SJ. The characterization of a new pale blue corrosion product found on copper alloy artifacts. Stud Conserv. 2002;47(4):217–27.
55. Ingo GM, Angelini E, de Caro T, Bultrini G, Calliari I. Combined use of GDOES, SEM-EDS, XRD, and OM for the microchemical study of the corrosion products on archaeological bronzes, Applied Physics A. Mater Sci Process. 2004;79:199–204.
56. Sherif EM, Abbas AT, Halfa H, El-Shamy AM. Corrosion of high strength steel in concentrated sulfuric acid pickling solutions and its inhibition by 3-amino-5-mercapto-1, 2, 3-triazole. Int J Electrochem Sci. 2015;10:1777–91.
57. Farag HK, El-Shamy AM, Sherif EM, El-Abedin SZ. Sonochemical Synthesis of Nanostructured ZnO/Ag Composites in an Ionic Liquid. Z Phys Chem. 2016;230(12):1733–44. https://doi.org/10.1515/zpch-2016-0777.
58. Gallese F, Laguzzi G, Luvidi L, Ferrari V, Takacs S, Venturi G, Cesa P. A comparative investigation into the corrosion of different bronze alloys suitable for outdoor sculptures. Corros Sci. 2008;50:954–61.
59. Lucey VF. Development leading to the present understanding of the mechanism of pitting corrosion of copper. Br Corros J. 1972;7:36–41.
60. El-Shamy AM, Shehata MF, Metwally HIM, Melegy A. Corrosion and corrosion inhibition of steel pipelines in montmorilonitic soil filling material. Silicon. 2018;10(6):2809–15. https://doi.org/10.1007/s12633-018-9821-4.
61. Abd Elkarim AM, El-Shamy AM, Megahed MM, Kalmouch A. Evaluation of the inhibition efficiency of a new inhibitor on leaded bronze statues from Yemen. ARCTIC Journal. 2018;71(1):2–33.
62. Wang J, Xu C, Lu G. Formation processes of CuCl and regenerated Cu crystals on bronze surfaces in neutral and acidic media. Appl Surf Sci. 2006;252:6294–303.
63. Gettens RJ. Mineral alteration products of ancient metal objects, recent advances in conservation, London. Butterworths. 1963;90:89.
64. Eessaa AK, El-Shamy AM, Reda Y. Fabrication of commercial nanoporous alumina by low voltage anodizing. Egypt J Chem. 2018;61(1):175–85. https://doi.org/10.21608/ejchem.2017.2189.1175.
65. El-Shamy AM, Abdelfattah I, Elshafie OI, Shehata MF. Potential removal of organic loads from petroleum wastewater and its effect on the corrosion behavior of municipal networks. J Environ Manag. 2018;219:325–31. https://doi.org/10.1016/j.jenvman.2018.04.074.
66. Franke WA, Mircea M. Plutarch's report on the blue patina of bronze statues at Delphi: a scientific explanation. J Am Inst Conserv. 2005;44(2):103–16.
67. Scott DA. Copper and bronze in art, corrosion, colorants, conservation, getty conservation institute, Los Angeles. USA. 2002;108:124.
68. El-Kashef E, El-Shamy AM, Abdo A, Gad EAM, Gado AA. Effect of magnetic treatment of potable water in looped and dead-end water networks. Egypt J Chem. 2019;62(8):1467–81. https://doi.org/10.21608/ejchem.2019.7268.1595.
69. Abbas MA, Zakaria K, El-Shamy AM, El-Abedin SZ. Utilization of 1-butylpyrrolidinium chloride ionic liquid as an eco-friendly corrosion inhibitor and biocide for oilfield equipment: combined weight loss, electrochemical and SEM studies. Z Phys Chem. 2019;235(4):377–406. https://doi.org/10.1515/zpch-2019-1517.
70. Barrero CA, Morales AL, Mejia MI, Arroyave CE. On magnetite formation as a corrosion product of steel hyperfine interactions (C). In: Thomas MF, Williams JM, Gibb TC, editors. Proceedings of the international conference on the applications of the Mössbauer effect. Oxford: ICAME 2001; 2001.
71. Blackney K, Martin B. Development, and long-term testing of methods to clean and coat architectural wrought ironwork located in a marine environment, In Research and case studies in architectural conservation, Metals, 1.1998.
72. Shehata MF, El-Shafey S, Ammar NA, El-Shamy AM. Reduction of Cu^{+2} and Ni^{+2} ions from wastewater using mesoporous adsorbent: effect of treated wastewater on corrosion behavior of steel pipelines. Egypt J Chem. 2019;62(9):1587–602. https://doi.org/10.21608/ejchem.2019.7967.1627.
73. Zohdy KM, El-Shamy AM, Gad EAM, Kalmouch A. The corrosion inhibition of (2Z,2'Z)-4,4'-(1,2-phenylene bis (azanediyl)) bis (4-oxobut-2-enoic acid) for carbon steel in acidic media using DFT. Egypt J Pet. 2019;28(4):355–9. https://doi.org/10.1016/j.ejpe.2019.07.001.
74. Degrigny C. The search for new and safe materials for protecting metal objects. In: Argyropoulos V, editor. Metals and museums in the mediterranean, protection, preserving and interpreting. Athens: PROMET Project; 2008.

75. Dillmann P, Mazaudier F, Hoerle S. Advances in understanding atmospheric corrosion of iron I—rust characterization of ancient ferrous artifacts exposed to indoor atmospheric corrosion. Corros Sci. 2004;46(6):1401.

76. Reda Y, El-Shamy AM, Zohdy KM, Eessaa AK. Instrument of chloride ions on the pitting corrosion of electroplated steel alloy 4130. Ain Shams Eng J. 2020;11:191–9. https://doi.org/10.1016/j.asej.2019.09.002.

77. Reda Y, Zohdy KM, Eessaa AK, El-Shamy AM. Effect of plating materials on the corrosion properties of steel alloy 4130. Egypt J Chem. 2020;63(2):579–97. https://doi.org/10.21608/ejchem.2019.11023.1706.

78. Hammouch H, Dermaj A, Goursa M, Hajjaji N, Srhiri A. New Corrosion Inhibitor Containing Opuntia ficus indica Seed Extract for Bronze and Iron-based Artefacts, In Argyropoulos V, Hein A, Abdel Harith M (eds) Strategies for Saving our Cultural Heritage. Proceedings of the International Conference on Conservation Strategies for Saving Indoor Metallic Collections, Cairo. TEI of Athens. 2007.

79. Hoerle S, Mazaudie F, Dillmann PH, Santarini G. Advances in understanding atmospheric corrosion of iron. II. Mechanistic modeling of wet–dry cycles. Corros Sci. 2004;46:1431.

80. Shehata MF, El-Shamy AM, Zohdy KM, Sherif ESM, El Abedin SZ. Studies on the antibacterial influence of two ionic liquids and their corrosion inhibition performance. Appl Sci. 2020;10(4):1444. https://doi.org/10.3390/app10041444.

81. El-Shamy AM, El-Hadek MA, Nassef AE, El-Bindary RA. Optimization of the influencing variables on the corrosion property of steel alloy 4130 in 35 wt% NaCl solution. J Chem. 2020. https://doi.org/10.1155/2020/9212491.

82. Ingo GM. Surface studies of patinas and metallurgical features of uncommon high-tin bronze artifacts from the Italic necropolises of ancient Abruzzo (Central Italy). Appl Surf Sci. 2019;470:74.

83. Fonseca LRC, Mateus T, Dias AA, Sequeira A, Cardoso A. Conservation of bronze artifacts by laser cleaning and protective coatings. J Cult Herit. 2018;33:92–100.

84. Monnier J, Burger E, Berger P, Neff D, Guillot I, Dillmann Ph. Localization of oxygen reduction sites in the case of iron long-term atmospheric corrosion. Corros Sci. 2011;53:2468.

85. El-Shamy AM, El-Hadek MA, Nassef AE, El-Bindary RA. Box-Behnken design to enhance the corrosion resistance of high strength steel alloy in 35 wt% NaCl solution. Mor J Chem. 2020;8(4):788–800. https://doi.org/10.48317/IMIST.PRSM/morjchem-v8i4.21594.

86. El-Shamy AM. A review on biocidal activity of some chemical structures and their role in mitigation of microbial corrosion. Egypt J Chem. 2020;63(12):5251–67. https://doi.org/10.21608/ejchem.2020.32160.2683.

87. Oudbashi O. From excavation to preservation: preventive conservation approaches in archaeological bronze collections, wallon. 2015.

88. Oudbashi O. Investigation on corrosion stratigraphy and morphology in some iron age bronze alloys vessels by OM, XRD, and SEM–EDS methods. Applied Physics A. 2016. https://doi.org/10.1007/s00339-016-9793-4.

89. Eessaa AK, El-Shamy AM. Review on fabrication, characterization, and applications of porous anodic aluminum oxide films with tunable pore sizes for emerging technologies. Microelectron Eng. 2023;279: 112061. https://doi.org/10.1016/j.mee.2023.112061.

90. El-Bindary R, El-Shamy AM, Elhadek MA, Nassef A. Statistical analysis of the inhibition of carbon steel corrosion in 3.5 wt. % NaCl solution using Lawsonia extract. Port-Said Eng Res J. 2021;25(1):101–13. https://doi.org/10.21608/pserj.2020.35020.1050.

91. Zohdy KM, El-Sherif RM, El-Shamy AM. Corrosion and passivation behaviors of tin in aqueous solutions of different pH. J Bio Tribo-Corros. 2021;7(2):1–7. https://doi.org/10.1007/s40735-021-00515-6.

92. Pan C, et al. Atmospheric corrosion of copper exposed in a simulated coastal-industrial atmosphere. J Mater Sci Technol. 2016;33(6):587.

93. Petiti C, et al. Effects of cleaning procedures on the long-term corrosion behavior of bronze artifacts of the cultural heritage in the outdoor environment. Environ Sci Pollut Res. 2020. https://doi.org/10.1007/s11356-020-07814-4.

94. Selwyn L. Overview of archaeological iron: the corrosion problem, key factors affecting treatment, and gaps in current knowledge, In Ashton, J. and Hallam D. (Eds) Metal 2004: Proceedings of interim meeting of the ICOM-CC Metal WG, National Museum of Australia Canberra. 2004.

95. El-Shamy AM, Abdel Bar MM. Ionic liquid as water soluble and potential inhibitor for corrosion and microbial corrosion for iron artifacts. Egypt J Chem. 2021;64(4):1867–76. https://doi.org/10.21608/ejchem.2021.43786.2887.

96. Zohdy KM, El-Sherif RM, Ramkumar S, El-Shamy AM. Quantum and electrochemical studies of the hydrogen evolution findings in corrosion reactions of mild steel in acidic medium. Upstream Oil Gas Technol. 2021;6: 100025. https://doi.org/10.1016/j.upstre.2020.100025.

97. Shashoua Y, Matthiesen H. Protection of iron and steel in large outdoor industrial heritage objects. Corros Eng Sci Technol. 2010;45(5):357.

98. Sik PJ. The technological and social implication of the discriminated use of tin and arsenic noted in EIA copper-based objects of Central Kazakhstan, Archaeological and Anthropological Sciences. 2020.

99. Elsayed EM, Eessaa AK, Rashad MM, El-Shamy AM. Preparation and characterization of ZnO thin film on anodic Al_2O_3 as a substrate for several applications. Egypt J Chem. 2022;65(10):119–29. https://doi.org/10.21608/ejchem.2022.110382.5021.

100. Sobhy DR. Study of corrosion mechanism of iron artifacts found in a chloride-rich environment and the methods of chloride removal, with application on selected objects, Ph.D., Conservation department, Faculty of Archaeology, Cairo University. 2014.

101. Stratmann M. The atmospheric corrosion of iron and steel, Metallurgica I Odlewnictwo, 1990; 16(1).

102. Grosby AF, Young Lee J. Polymer nanocomposites: the nano effect on mechanical properties. J Polym Rev. 2007;47(2):217–29.

103. Aki Kutvanon A, Rossi G, Puisto SR, Rostedt NKJ, Ala- Nissla T. Influence of nanoparticle size, loading, and shape on the mechanical properties of polymer nanocomposites. J Chem Phys. 2012;137(21):214901–8.

104. Cheng Ma P, Jk K, Tang BZ. Effects of silane functionalization on the properties of carbon nanotube/epoxy nanocomposites. Compos Sci Technol. 2007;67(14):2965–72.

105. Ciprati DL. Mechanical characterization of polymer nanocomposites, and the role of interface. Master thesis of science in materials science and engineering, Georgia Institute of Technology. 2004.

106. Ciprati DL, Jacob K, Tannenbaum R. Characterization of polymer nanocomposite interphase and its impact on mechanical properties. Macromolecules. 2006;39(19):6565–73.

107. Davis J. Corrosion: understanding the basis library of congress. Almere: ASM International; 2000.

108. Dinari M, Reza Raja A. Structural thermal and mechanical properties of polymer nanocomposites based on organo soluble polyamide with naphtyl pendent group layered double hydroxide high performance. Polym J. 2017;29(8):951–9.

109. Fedel M. Environmentally friendly hybrid coatings for corrosion protection: Saline based pretreatments and nanostructured waterborne coatings, department of materials engineering and industrial technologies, University of Toronto, Italy, 2010; 7-10.

110. Shehata MF, El-Shamy AM. Hydrogen-based failure in oil and gas pipelines a review. Gas Sci Eng. 2023;115: 204994. https://doi.org/10.1016/j.jgsce.2023.204994.

111. Figueiredo E. Study of metallurgy and corrosion of ancient copper-based artifacts from the Portuguese territory, Universidad Nova de Lisboan, Faculdade de cienciase Technologia. 2010.

112. Eessaa AK, Elkady OA, El-Shamy AM. Powder metallurgy as a perfect technique for preparation of Cu-TiO$_2$ composite by identifying their microstructure and optical properties. Sci Rep. 2023;13(1):7034. https://doi.org/10.1038/s41598-023-33999-y.

113. Helmi FM. Study of color conversion by time in ancient Egyptian faience artifacts. Sci Culture. 2016;2(3):17–23.

114. Nogueira RA, Gonçalves JP, Pinto AM, Pinto HM, Montemor MF. Surface preparation and corrosion protection of bronze artifacts using sol-gel coatings. J Coat Technol Res. 2019;16(1):119–28.

115. De Santis E, de Carvalho ML, Iannuccelli S, Pelosi C, Sgamellotti A, Marabelli M. Development of a multi-step conservation strategy for bronze artifacts from the underwater cultural heritage. Herit Sci. 2019;7(1):1–16. https://doi.org/10.1186/s40494-019-0334-0.

116. Borgia G, Pelosi C, Romani A, Cantisani E, Santamaria U, Iacobucci G, Zanoni R. Characterization of corrosion products on bronze artifacts from the underwater cultural heritage, and the development of a conservation strategy. Stud Conserv. 2018;63(4):207–19. https://doi.org/10.1080/00393630.2017.1407060.

117. Shoji T. Factors affecting stress corrosion cracking (SCC) and fundamental mechanistic understanding of stainless steels. In Stress Corrosion Cracking, Woodhead Publishing Series in metals and surface engineering. 2011.

118. Ciprati DL. Mechanical characterization of polymer nanocomposites, and the role of interface. Master's thesis of science in materials science and Engineering, Georgia Institute of Technology. 2004.